Estuaries and Coasts (2024) 47:1012–1031
https://doi.org/10.1007/s12237-024-01334-x

Improving Satellite Chlorophyll-a Retrieval in the Turbid Waters of the Bay of Fundy, Canada

Kristen L. Wilson[1] · Andrea Hilborn[2] · Stephanie Clay[1] · Emmanuel Devred[1]

Received: 28 September 2023 / Revised: 30 January 2024 / Accepted: 7 February 2024 / Published online: 15 March 2024

Abstract
The Bay of Fundy is a highly productive ecosystem within the Northwest Atlantic where extreme tides and strong currents result in a large gradient of sediment concentrations across and along the bay. We processed daily satellite data from the MODerate resolution Imaging Spectroradiometer (MODIS) on the Aqua satellite from 2003 to 2021 at 300-m resolution to understand and quantify spatial and temporal trends in chlorophyll-a concentration (chl-a, a measure of phytoplankton biomass), and suspended particulate matter concentration (SPM) in the Bay of Fundy surface waters. To account for high sediment loading (up to 100's g m^{-3}) and moderate chl-a (median in situ chl-a of 1.5 mg m^{-3} from 2003 to 2021), coefficients of the OC3M chl-a algorithm were regionally tuned using in situ chl-a data, and satellite-derived SPM was incorporated within the chl-a retrieval algorithm to account for possible bias. The updated new algorithm was denoted as $OC_{X\text{-}SPMCor}$. Chl-a computed using $OC_{X\text{-}SPMCor}$ showed better performance against in situ chl-a than the generic OC3M with a coefficient of determination that increased from 0.01 to 0.28 and a root mean square logarithmic error that decreased by 35%. Unlike previous remote sensing studies, $OC_{X\text{-}SPMCor}$ correctly predicted the particular chl-a seasonality in the Bay of Fundy, which does not follow the typical occurrence of spring/fall blooms as observed in the adjacent Gulf of Maine and Scotian Shelf. For the first time, satellite-predicted chl-a aligned with the phenology of in situ chl-a, where chl-a continually increased from April to June and remained high all summer, with a small secondary summer peak before decreasing in the fall. SPM seasonality followed an opposite trend where SPM reached a maximum in winter and a minimum in summer. A small number of matchups and high temporal variability on the hourly time scale precluded a robust assessment of the satellite-derived SPM. However, comparisons between time series of remotely sensed and in situ SPM demonstrated the ability of the satellite-derived SPM to capture temporal variations, though the absolute values may be slightly underestimated. Accurate maps of phytoplankton biomass and sediment concentrations are essential variables required for effective management and conservation of marine ecosystems in the Bay of Fundy.

Keywords Chlorophyll-a · MODIS Aqua · Ocean color · Regional calibration · Remote sensing · Suspended particulate matter

Introduction

The Bay of Fundy is a temperate bay in the Northwest Atlantic that is characterized by an extreme tidal range upwards of 16 m (Garrett 1972), and strong currents exceeding 5 m s^{-1} (Mulligan et al. 2019), which drive extremely high sediment concentrations through sediment resuspension (Amos and Topliss 1985; Dalrymple et al. 1990; Zions et al. 2017; Mulligan et al. 2019). Water enters the Bay of Fundy along the Nova Scotian coastline, and flows in a counterclockwise direction, exiting along the New Brunswick coastline, either entering the Gulf of Maine west of Grand Manan Island or persisting within

Communicated by Brian B. Barnes

✉ Kristen L. Wilson
kristen.wilson@dfo-mpo.gc.ca

[1] Fisheries and Oceans Canada, Bedford Institute of Oceanography, Dartmouth, NS, Canada

[2] Fisheries and Oceans Canada, Institute of Ocean Sciences, Sidney, BC, Canada

the Fundy gyre located east of Grand Manan Island (Fader et al. 1977; Aretxabaleta et al. 2008; Aretxabaleta et al. 2009) (Fig. 1). The Saint John River is the largest freshwater input into the Bay of Fundy, which creates a notable dark plume off Saint John, New Brunswick, and flows in spring which are ~6 times greater than the winter/summer ones (Toodesh 2007). Tidal forces and dominant currents push this plume southwest along the New Brunswick coast. The strong tidal forcing makes the Bay of Fundy an ideal test area for generating tidal power (Greenberg and Amos 1983; Ashall et al. 2016). The bay is also a highly productive ecosystem which supports several commercial fisheries (Rozalska and Coffen-Smout 2020). While the large tidal range and turbid waters limit the distribution of submerged vegetation such as kelp and seagrass, extensive salt marshes are distributed along the coastline (Virgin et al. 2020; Rabinowitz et al. 2023), which play important roles in shoreline buffering, habitat provision, and carbon storage (Minello et al. 2003; McLeod et al. 2011; Möller et al. 2014). The Musquash Estuary along the Northwest coast is one such salt marsh which has been designated as a Marine Protected Area due to its pristine condition (Oceans and Coastal Management Division Fisheries and Oceans Canada 2017). Several other biological and ecologically significant areas have also been noted within the Bay of Fundy due to significant marine mammal and bird aggregations, important lobster habitat, cold water corals, horse mussel reefs, and large intertidal mudflats which support diverse invertebrate populations (Buzeta 2014). Recognizing the importance of this ecosystem, it is critical

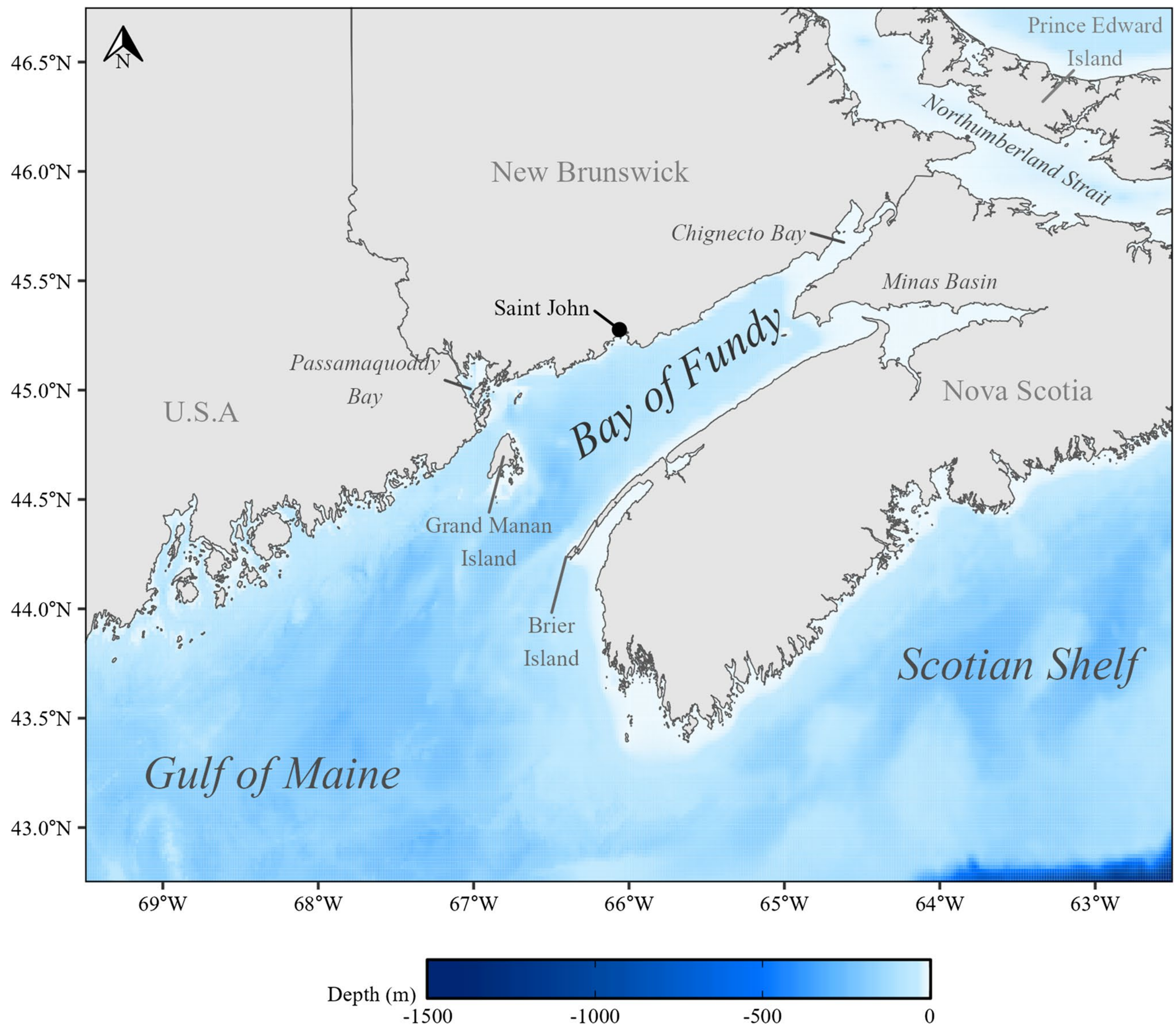

Fig. 1 Bay of Fundy study area in the Northwest Atlantic showing bathymetry and notable landmarks around the bay.

to understand the large-scale oceanographic trends within the Bay of Fundy to support management of the region.

One tool for understanding and quantifying large-scale trends in sediment dynamics and phytoplankton phenology is satellite remote sensing. Within the Bay of Fundy, satellite remote sensing efforts to understand sediment dynamics have so far been focused on the Minas Basin and Chignecto Bay regions (Amos and Alfoldi 1979; Amos and Long 1980; Amos and Asprey 1981; Greenberg and Amos 1983; Tao et al. 2014). These two areas are located in the upper forks of the Bay (Fig. 1) and correspond to the highest sediment concentrations ranging from < 1 to 100's g m^{-3} depending on the time of year and tidal height (Amos and Topliss 1985; Zions et al. 2017). These high sediment concentrations are driven by tidal currents, resuspension of bottom sediment from wind-induced mixing, and wave action (Dalrymple et al. 1990). Satellite remote sensing has also been used at large scales across the Gulf of Maine, including the Bay of Fundy and Scotian Shelf, to understand chlorophyll-a concentration (chl-a), a proxy for phytoplankton biomass, and sea-surface temperature dynamics (Li and He 2014; Devred et al. 2018; Fuentes-Yaco et al. 2020). While one study was interested in developing warning systems for harmful algal blooms within the Bay of Fundy (Devred et al. 2018), to date such efforts have relied on chl-a estimates computed using generic, globally calibrated chl-a algorithms. However, satellite remote sensing of chl-a is challenging in this region as the significant tidal range within the Bay of Fundy results in large fluctuations of sediment concentration over the course of a single day, or even hour. As such, even compared to other complex coastal waters, the optical characteristics of the Bay of Fundy reduce the accuracy of generic algorithms, as the high sediment load drives the remotely sensed optical signal, which manifests as an overestimation of chl-a retrievals. While no regional chl-a algorithm has yet been developed for the Bay of Fundy, regional chl-a algorithms have been developed for the Northwest Atlantic (Clay et al. 2019) and the Gulf of St Lawrence (Laliberté et al. 2018; Laliberté and Larouche 2023), which are strongly impacted by colored dissolved organic matter (CDOM), as opposed to sediment. In these areas, the mean error of chl-a retrieval was reduced by an order of magnitude following the development of the regional algorithms.

Satellite remote sensing has successfully been applied in other highly turbid environments to retrieve chl-a using a variety of techniques that exploit the relationship between different spectral bands. In the Arctic Ocean, the blue-green ratio algorithm was recalibrated with a large in situ database to account for the low sun elevation, different phytoplankton bio-optical characteristics due to adaptations to an extreme light environment, and relatively high levels of CDOM (Lewis and Arrigo 2020). Yet in regions with high sediment loading, such as the shelf region impacted by the direct outflow of the Mackenzie River where sediment concentrations regularly exceed 10 g m^{-3} (Doxaran et al. 2015), chl-a may still be overestimated (Hilborn and Devred 2022). Elsewhere in the Atlantic Ocean, using red/near-infrared (NIR) algorithms with narrow band ranges, chl-a retrievals were improved in the Río de la Plata estuary (Dogliotti et al. 2021) where suspended particulate matter concentrations (SPM) range from 10 to 100's g m^{-3} (Camiolo et al. 2019). In the turbid Chesapeake Bay of the northeastern USA, red-edge chl-a algorithms were generally superior at estimating high chl-a (i.e., > 10 mg m^{-3}); however, in the upper reaches of the bay where sediment concentrations were highest, and for lower chl-a, blue-green band ratio algorithms performed better (Wynne et al. 2022). Consequently, the application of satellite remote sensing in turbid environments with highly variable sediment and chl-a requires careful consideration to accurately quantify sediment and phytoplankton dynamics.

To help understand the complex dynamics of sediment distribution and phytoplankton biomass in the turbid Bay of Fundy, we examined the time series of chl-a and SPM from 2003 to 2021 by processing data from the MODerate resolution Imaging Spectroradiometer (MODIS) sensor on the Aqua satellite. We developed a regionally tuned chl-a algorithm calibrated using a database of in situ chl-a and SPM to account for the possible impact of SPM on chl-a retrieval. The satellite data were meticulously quality controlled to evaluate the extent to which one can trust these products in the Bay of Fundy. We produced daily, seasonal, annual, and climatology time series and maps of chl-a and SPM on a 300-m grid. Such data layers are needed in order to be able to understand sediment dynamics and phytoplankton phenology across temporal and spatial scales.

Methods

In Situ Chl-a and SPM

The in situ chl-a dataset included the Western Isles phytoplankton monitoring program (Martin et al. 2014) and the Biological and Chemical databases (Devine et al. 2014; BIOCHEM, https://www.dfo-mpo.gc.ca/science/data-donnees/biochem/index-eng.html, accessed on August 16, 2022). The most abundant in situ chl-a measurements within DFO databases consist of extracted chl-a measured with a benchtop Turner fluorometer (referred to hereafter as "Turner chl-a"). Turner chl-a measurements have repeatedly been acquired across the Bay of Fundy for all years of interest (2003–2021; Fig. 2). These measurements are collected following the Atlantic Zone Monitoring Program (AZMP) protocol (Mitchell et al. 2002) which uses the Holm-Hansen et al. (1965) method for calculating chl-a. Briefly, 100 mL of seawater was collected by rosette

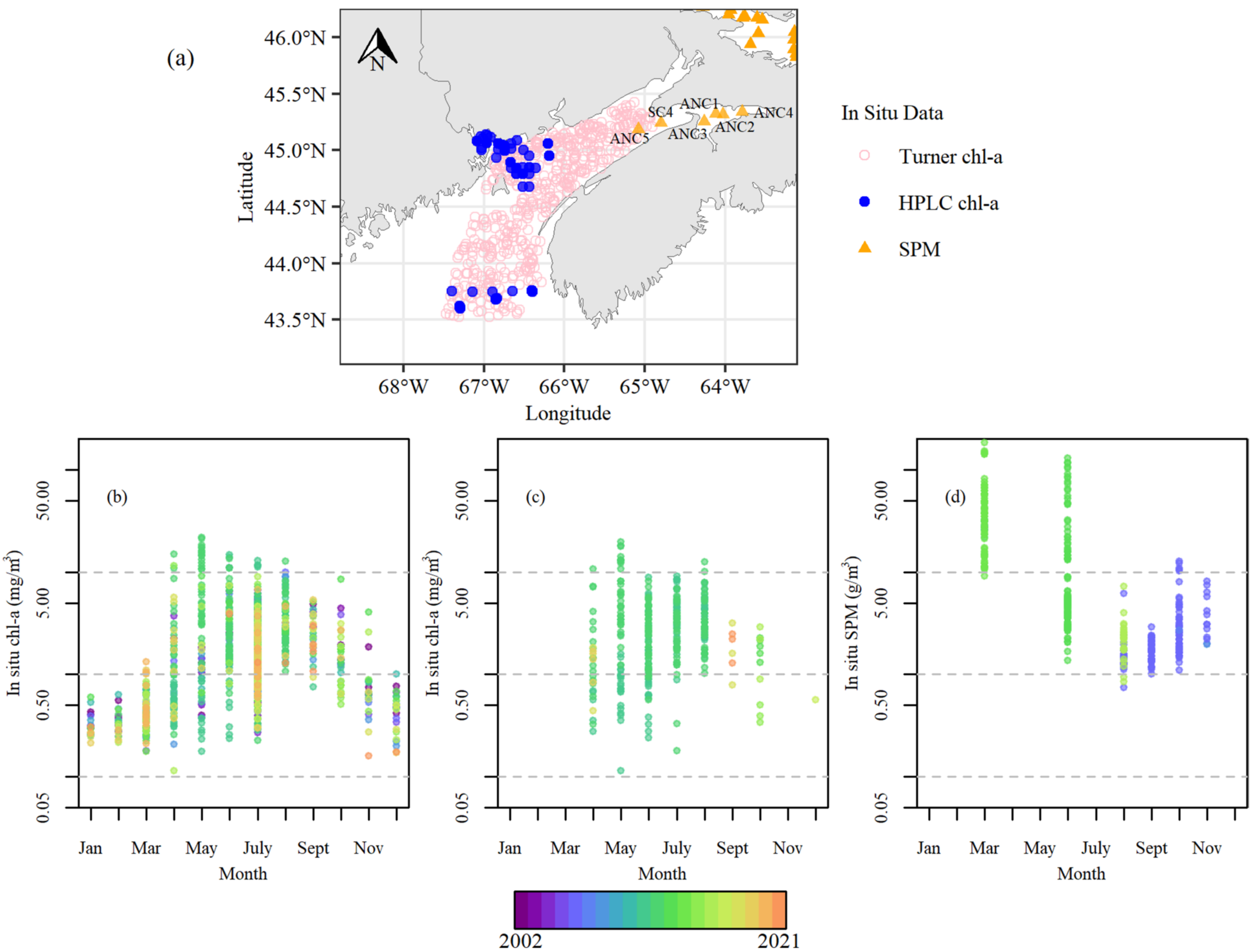

Fig. 2 Study region showing the location of Bay of Fundy, Canada, with the limits denoting the region used for the MODIS imagery (**a**). Locations of ship-based measurements and type are indicated with the corresponding time series from 2002 to 2021 for Turner-derived chl-a (**b**), HPLC-derived chl-a (**c**), and SPM (**d**). Horizontal light grey dashed lines indicate thresholds of 0.1, 1, and 10 for the respective measurements; note the log-10 scale of the *y* axis. HPLC-derived chl-a collection began in 2011 whereas Turner-derived chl-a was available across all years. SPM station names from Fig. 3 are labelled.

and was immediately filtered onto a 25 mm GF/F filter. The filters were extracted in 10 mL of 90% acetone in the dark for 24 h at −20 °C. The extracted chl-a fluorescence is then measured with a Turner fluorometer and converted to chl-a concentration using calibration coefficients calculated at the Bedford Institute of Oceanography. High Performance Liquid Chromatography (HPLC) chl-a have also been collected in the region, albeit across a limited spatial and temporal range ($n = 318$; Fig. 2). The HPLC samples were simultaneously collected with Turner chl-a, albeit with a larger volume of filtered seawater from 500 to 1000 mL, and were immediately flash-frozen and held at −80 °C until analysis at a later date. The detailed chl-a matchup analysis in our study (see below) used Turner-derived chl-a given their greater number and better spatial-temporal coverage than HPLC-derived chl-a (Fig. 2). HPLC-derived chl-a were not used for matchups but instead were used to ensure the correct seasonal representation and magnitude of Turner-derived chl-a. All chl-a data, both Turner and HPLC, were collected within 10 m of the surface.

We compiled in situ SPM collected during two oceanographic cruises that took place in the Minas Basin in June 2013 and March 2014, during which SPM was sampled at fixed stations repeatedly over a full tidal cycle (see Fig. 1B in Horne and Law 2013; Zions et al. 2017). This dataset showed a strong gradient of SPM from west to east, and a strong seasonal cycle with higher SPM in March relative to June. The median surface (< 10 m) SPM in the Minas Basin was 31.9 g m^{-3} in March compared to 5.0 g m^{-3} in June (Fig. 2). All SPM data were collected within 10 m of the surface.

Satellite Data and Processing

Satellite imagery acquired by the MODIS sensor on the Aqua satellite (MODIS-Aqua; hereafter MODIS) operated and distributed by the National Aeronautics and Space Administration (NASA) was used in this study. MODIS was launched in 2002, and images were processed for the years 2003 to 2021, corresponding to all years with a complete time series. Individual Level 1A images (L1A, uncorrected radiance) were downloaded from the NASA Ocean Biology Processing Group (OBPG; https://oceancolor.gsfc.nasa.gov/), for a spatial box bounded by 43.1–46.2 °N and 68.8-63.1 °W (Fig. 2a), and processed using the freely available SeaDAS software (version 7.5.2.1, https://seadas.gsfc.nasa.gov/). The L1A images were corrected for atmospheric effects and converted to remote-sensing reflectance (R_{rs}) using the NIR-SWIR switching algorithm (Wang and Shi 2007), which performed well in other regions with high SPM (Doxaran et al. 2015). Initial results were compared to the MUMM (Management Unit of the North Sea Mathematical Models; Ruddick et al. 2000) atmospheric correction (results not shown), which was found to produce R_{rs} with a low dynamic range of values and was therefore deemed less sensitive than the NIR-SWIR algorithm.

While two MODIS bands (659 and 865 nm) are acquired at a resolution of 250-m and two bands (470 and 555 nm) are acquired at a resolution of 500-m, the SeaDAS processing occurs at a 1-km resolution. We chose to process the Level 1A satellite data at 250-m resolution (l2gen option "resolution=250"), which was performed internally in SeaDAS by bilinearly interpolating each 1-km pixel into 16 sub-pixels (e.g., Franz et al. 2006), to better align with the complex coastline and oceanographic features of the Bay of Fundy. Following interpolation, the integrated SeaDAS land mask at 250-m was used after comparing it to a coastline shapefile to remove any land pixels. In the future a buffered coastline should be used to remove any interpolated pixels that would originally have intersected land. Pixels with a nominal resolution of 1-km may still be contaminated by land-adjacency effects when bi-linearly interpolated on a 250-m grid. Although the coastline was not buffered before collecting matchups, this did not affect any of the matchups around the Prince 5 station (See *Chl-a Matchups*).

Numerous quality-control flags were applied in order to filter out low- or suspicious-quality pixels (Table S1 in Supplementary Materials 1), and pixels with negative reflectance values in bands 9 to 13 were removed from further analysis (Table 1). When multiple images overlapped the study region on a given day, they were aggregated into a single daily composite by aligning the images onto a common 300-m resolution grid to reduce data gaps and calculating the median value at each grid cell using the Generic Mapping Tools (GMT) software (https://www.generic-mapping-tools.org/). A slight increase in pixel size is recommended when switching to a standard grid to reduce data gaps from off-nadir pixels, hence the increase from 250 to 300-m. Small gaps may persist in images acquired at an angle from nadir (e.g., Moiré pattern); in this study, we chose not to fill these small gaps, while other studies or reprojection programs can reduce them through interpolation. All further analysis was performed using R version 4.2 (R Core Team 2021).

SPM and Chl-a Algorithms

SPM was calculated using the single red band equation developed by Nechad et al. (2010) with wavelength-specific coefficients derived for band 13 (Table 1):

$$SPM = \frac{A^{\rho} \times R_{rs}(\lambda_{red})}{1 - (R_{rs}(\lambda_{red}) \times C^{\rho})} \quad (1)$$

where C^{ρ} and A^{ρ} are two calibration parameters and SPM is expressed in g m^{-3}. The first parameter was calibrated using standard inherent optical properties, the latter from non-linear regression of SPM data on reflectance. Both parameters have standard published values for MODIS

Table 1 Algorithm coefficients and references for chl-a and SPM algorithms used in this study. Note that OC3M coefficients were from the R2018 version.

Algorithm	Coefficients	Band no. and range (nm)	Reference
OC3M	$a_0 = 0.2424$ $a_1 = -2.7423$ $a_2 = 1.8017$ $a_3 = 0.0015$ $a_4 = -1.2280$	Band 9 (blue, 438–448) Band 10 (blue, 483–493) Band 12 (green, 546–556)	https://oceancolor.gsfc.nasa.gov/resources/atbd/chlor_a/
Nechad	$A^{\rho} = 362.09$ $C^{\rho} = 0.1736$	Band 13 (red, 662–672)	Nechad et al. 2010
$OC_{X\text{-}SPMCor}$	$a_0 = -0.2307818$ $a_1 = -2.8174856$ $a_2 = -0.9109887$ $a_3 = 1.9070607$ $a_4 = 1.3149395$ $a_{spm} = -1.0019175$	Band 10 (blue, 483–493) Band 12 (green, 546–556) Band 13 (red, 662–672)	This study

bands (Nechad et al. 2010). Another study showed good performance of SPM retrieval across large gradients of SPM when using a red-centered band (Ody et al. 2016).

Two methods were used to derive chl-a. First, chl-a was calculated using the OC3M blue-green band ratio (O'Reilly et al. 1998) with published coefficients calibrated for MODIS (Table 1), where the blue band (9 or 10) is selected to maximize the blue-to-green ratio, R_{OCx}:

$$R_{OCx} = \log_{10}\left(max\left(\frac{R_{rs}(\lambda_{blue})}{R_{rs}(\lambda_{green})} \right) \right) \tag{2}$$

R_{OCx} (Eq. 2) is inputted into the following polynomial equation to infer chl-a:

$$\log_{10}(chl\text{-}a) = a_0 + a_1 R_{OCx} + a_2 R_{OCx}^2 + a_3 R_{OCx}^3 + a_4 R_{OCx}^4 \tag{3}$$

where chl-a is expressed in mg m^{-3}. Note that all mention of OC3M includes both bands 9, 10, and 12 in the band ratio calculation. NASA's standard OCI algorithm, which switches from OC3M to a different algorithm at low chl-a (Hu et al. 2012), was also tested but provided poor results in high SPM environments resulting in abrupt transitions in chl-a.

The OC3M generic algorithm provided poor chl-a retrievals (see *Chl-a matchups*). Therefore, a second chl-a algorithm was developed ($OC_{X\text{-}SPMCor}$). This algorithm updated the polynomial coefficients in Eq. 2 (i.e., a_0 to a_4) as described in Clay et al. (2019) using matchup data within the Bay of Fundy, and had a novel addition of a term to account for possible contamination of remote sensing reflectance by high SPM (Table 1). Here, the reflectance ratio (i.e., Eq. 2) was calculated using band 10 (blue) and 12 (green) only, and Eq. 1 was used to calculate SPM:

$$\log_{10}(chl\text{-}a) = a_0 + a_1 R_{OCx} + a_2 R_{OCx}^2 + a_3 R_{OCx}^3 + a_4 R_{OCx}^4 + a_{spm}\left(\log_{10} SPM\right) \tag{4}$$

Only bands 10 and 12 were used in the band ratio calculation (Eq. 2) for $OC_{X\text{-}SPMCor}$ for two reasons. First, the results were very similar whether band 9 was included or not. Second, this was consistent with other regional tuning studies in the Northwest Atlantic that found increased chl-a accuracy when the 443-nm band was excluded (Clay et al. 2019). Note that we tested several iterations of Eq. 4 with different exponents for the SPM term and using the $R_{rs}(\lambda_{red})$ directly instead of the calculated SPM value (results not shown here), but the current Eq. 4 provided the best chl-a retrievals compared to in situ matchups. For completeness, we also provide a limited discussion of $OC_{X\text{-}BoF}$ which represents Eq. 4 without the SPM term but still regionally tuned to the Bay of Fundy.

Matchups

Satellite matchup extraction was carried out on a 5 × 5 matrix centered on the in situ measurement. The in situ measurement was the topmost value measured within a profile and was always collected within 10 m of the surface. An in situ data point was considered a match if the sample was collected on the same calendar day as the satellite image acquisition. The center pixel always overlapped the in situ sampling location. The median value of the 5 × 5 box was used in further analysis if at least 5 valid pixels out of 25 were detected in the matrix. We also tested using the arithmetic and geometric means within the 5 × 5 box, which provided similar results when compared to the in situ measurement, but the median was less sensitive to outliers. Note that the satellite image had already been pre-screened for negative R_{rs} and several quality control flags as described in *Satellite Data & Processing* such that erroneous pixels were already excluded from any data analysis.

The new model coefficients for $OC_{X\text{-}SPMCor}$ (Table 1) and $OC_{x\text{-}BoF}$ (results not shown) were tuned using the entire dataset as input. Here, the 5 × 5 median $R_{rs}(\lambda)$ and satellite-predicted SPM were used as input to be consistent with the matchup analysis. To test the stability of the coefficients, the *boot* () function in R was used to calculate 95% confidence intervals for each optimized coefficient using BCA intervals (Davison and Hinkley 1997; Canty and Ripley 2022). Coefficients were optimized with an iterative procedure which forced the slope to one and intercept to zero for the linear regression between log-10 transformed satellite-derived and log-10 transformed in situ chl-a (O'Reilly et al. 1998; Clay et al. 2019). This forcing was done to ensure the preservation of the dynamic range of satellite-derived chl-a without introducing a bias. We explored tuning the coefficients without the forcing; however, this resulted in a loss of dynamic range which increased over- and underestimation of low and high chl-a, respectively, despite marginal increases in accuracy statistics.

To assess model accuracy, the root mean square logarithmic error (RMSLE) was calculated using the *rmse()* function in the R package *oceancolouR* (https://github.com/BIO-RSG/oceancolouR) on log-10 transformed data as in Clay et al. (2019). The mean absolute error (MAE) was also calculated using the *mae*() function in the R *Metrics* package (Hamner et al. 2022). Finally, the coefficient of determination (R^2), slope, and intercept were computed for the linear regression of log-10 transformed satellite-derived chl-a on log-10 transformed in situ chl-a using the Standard Major Axis method of Type 2 regression using the R *lmodel2()*

function from the package of the same name (Legendre 2022). Accuracy metrics were calculated for the entire dataset used for model training ($n = 174$), as well as the average accuracy metric following a 5-fold cross-validation which was repeated 10 times ($n = \sim 34$).

Limited SPM matchup data was available for the Bay of Fundy and no data from the Minas Basin cruises overlapped with cloud-free satellite data. Therefore, to validate our SPM time series, the median SPM from a 5 × 5 box centered on the sampling location was extracted from each daily composite for March and June (Fig. 2). In situ SPM was measured along a vertical profile and all measurements within the first 10 m were used (Horne and Law 2013; Zions et al. 2017). The daily median SPM was used to create a March and June climatology for two time periods: 2003–2021 and 2012–2014. These climatologies were compared to in situ measurements (Zions et al. 2017) to assess the performance of the satellite products across the tidal cycle. While this approach differs from matchup protocols, it provides information on the overall performance of the algorithm, i.e., its ability to capture the range and seasonality of SPM dynamics for the years in situ data was collected, and demonstrates the representativeness of these years (2012–2014) across the full time series. The same matchup procedure as chl-a was repeated for SPM data collected in the Northumberland Strait in 2006 (Fuentes-Yaco et al. 2020). While it is outside the Bay of Fundy, this area corresponds to another region of elevated SPM.

Results

SPM Matchups

In March 2012 and 2014, four stations were repeatedly sampled throughout a tidal cycle to observe changes in SPM within the Minas Basin (Fig. 2; Horne and Law 2013; Zions et al. 2017). SPM ranged from 9 to 183 g m^{-3}, and were highly variable within a day, and sometimes between a narrow depth range (2–5 m; Supplementary Materials 2 Figs. S1-2). While none of these observations met the temporal criteria (i.e., within 3 h of satellite pass) to complete a rigorous matchup, satellite-derived SPM agreed with the spatial-temporal variability of in situ values, however, with a systematic underestimation of absolute SPM (Fig. 3). ANC4 was the station closest to shore and no satellite data was

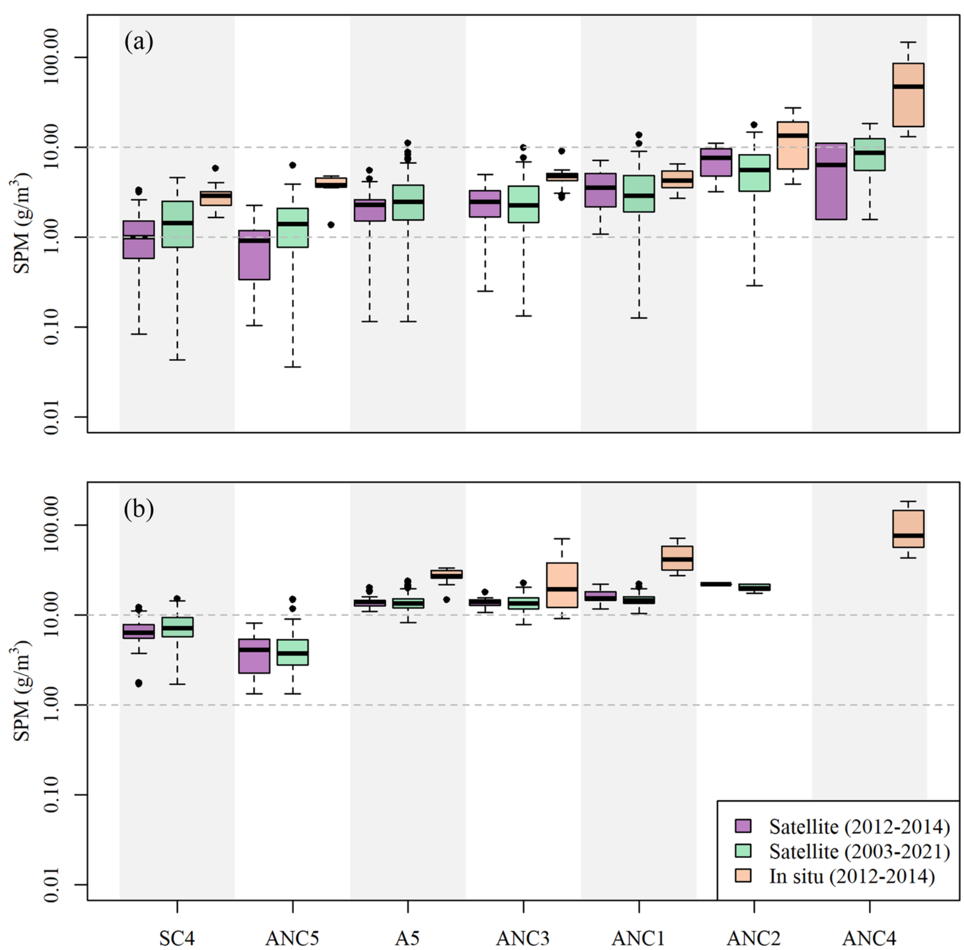

Fig. 3 Boxplots of the 5 × 5 median satellite-derived SPM and in situ SPM collected at seven fixed stations in June (**a**) and March (**b**) along a gradient of increasing SPM showing the temporal variability of SPM over select time periods. The satellite data was based on the median of a 5 × 5 box around the respective stations from 2003 to 2021, and 2012 to 2014 alone to temporally overlap with the in situ data. The in situ data was collected in March of 2012 or 2014, and June of 2013, and water samples within the upper 10 m of the water column were repeatedly sampled over a full tidal cycle (Horne and Law 2013; Zions et al. 2017).

available for this station in March due to ice coverage, and predicted SPM exceeded the Nechad et al. (2010) saturation threshold of 50 g m^{-3}. In June 2013, in situ measurements and satellite-derived SPM showed a strong spatial gradient but with lower concentrations than in March, again with an underestimation of satellite-derived SPM. SPM seasonal trends from 2012 to 2014 were representative of the entire 2003–2021 time series. Despite our limited matchup data, the relative change in SPM across the Bay of Fundy was an important factor to correct the chl-a algorithm.

The satellite-derived SPM data showed good agreement with the in situ SPM collected in the Northumberland Strait (Fig. 4) with a low RMSLE of 0.27 and a high coefficient of determination (R^2) of 0.72. The data largely followed the 1:1 line for satellite concentrations > 1 g m^{-3} and the highest deviation (i.e., underestimation) was observed at low SPM.

Chl-a Matchups

In situ data collected from several fixed stations and oceanographic cruises revealed large variations of chl-a in the surface waters of the Bay of Fundy, with values that increased by two orders of magnitude from 0.1 to 10 mg m^{-3} and a strong seasonal cycle (Fig. 2b). The Turner dataset showed a strong seasonal cycle of winter minimum and summer maximum of chl-a, with an annual median chl-a of 1.5 mg m^{-3} (n = 1106). The HPLC data (n = 318) suggested a similar summer range of chl-a (0.178–12.64 mg m^{-3}) as the Turner chl-a (0.225–12.88 mg m^{-3}). Cloud cover and data quality control limited the number of in situ measurements used for comparison such that only 16% of the Turner-derived (174/1106) and 12% of the HPLC-derived (38/318) chl-a met the criteria to be extracted as matchup data. Turner chl-a were used in the matchup analysis as they were available across all months, at a greater spatial coverage across the Bay of Fundy, with more than four times the number of HPLC-based chl-a available for matchups.

The incorporation of the SPM term ($OC_{X\text{-}SPMCor}$) increased the stability of the model coefficients, relative to a regionally tuned model without the SPM term ($OC_{X\text{-}BoF}$; Supplementary Materials 3 Fig. S3). $OC_{X\text{-}SPMCor}$ also had a lower RMSLE and MAE relative to OC3M and $OC_{X\text{-}BoF}$ (Fig. 5; Table 2). When the 5 × 5 median satellite-derived chl-a was plotted against in situ chl-a (Fig. 6), two clusters were apparent in the OC3M data where low SPM (< 1 mg m^{-3}, purple) had good chl-a retrieval, but when SPM increased (> 1 mg m^{-3}, blue to red), the satellite chl-a was overestimated relative to the Turner chl-a. For these initial OC3M chl-a matchups, the satellite-derived chl-a was close, but below the 1:1 line when SPM < 1 mg m^{-3}. However, when SPM increased, satellite-derived chl-a deviated from in situ measurements (Fig. 6a). This deviation based on SPM resulted in poor matchup statistics (R^2 = 0.01; RMSLE = 0.58; Table 2) for the OC3M algorithm. When the original OC3M algorithm coefficients were regionally tuned and a SPM-dependent term was included (thereafter referred to as $OC_{X\text{-}SPMCor}$), the relationship between satellite-derived and in situ chl-a greatly improved with a 28 times increase in the R^2 value and a reduction in RMSLE from 0.58 to 0.38 (Fig. 5). The overestimation of chl-a at high SPM was largely corrected with the new $OC_{X\text{-}SPMCor}$ algorithm resulting in a decrease of satellite-derived chl-a that were in good agreement with the in situ measurements (Fig. 6). This new algorithm might overcorrect chl-a at high SPM (> 10 g m^{-3}) resulting in erroneously low predicted chl-a, but this is difficult to confirm as only two matchup points corresponded to these elevated SPM. Regardless, incorrectly predicted high chl-a from OC3M in regions with the highest SPM (Figs. 6a and 7a) were now correctly predicted (i.e., low values) with the $OC_{X\text{-}SPMCor}$ algorithm (Figs. 6b

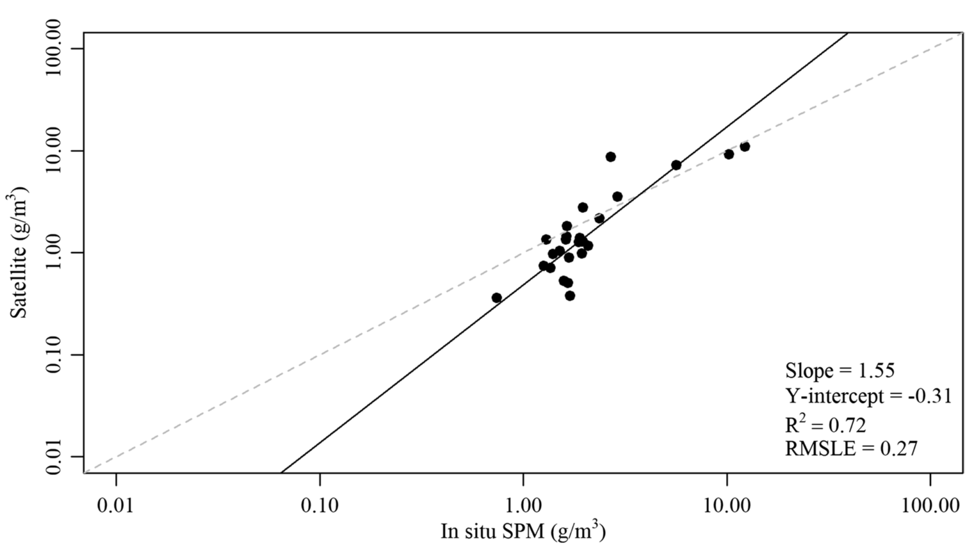

Fig. 4 Satellite matchups based on the Nechad SPM algorithm for data located in the Northumberland Strait from 2006 (Fuentes-Yaco et al. 2020). The 1:1 line is indicated with the grey dashed line and the solid black line is the regression of in situ versus satellite.

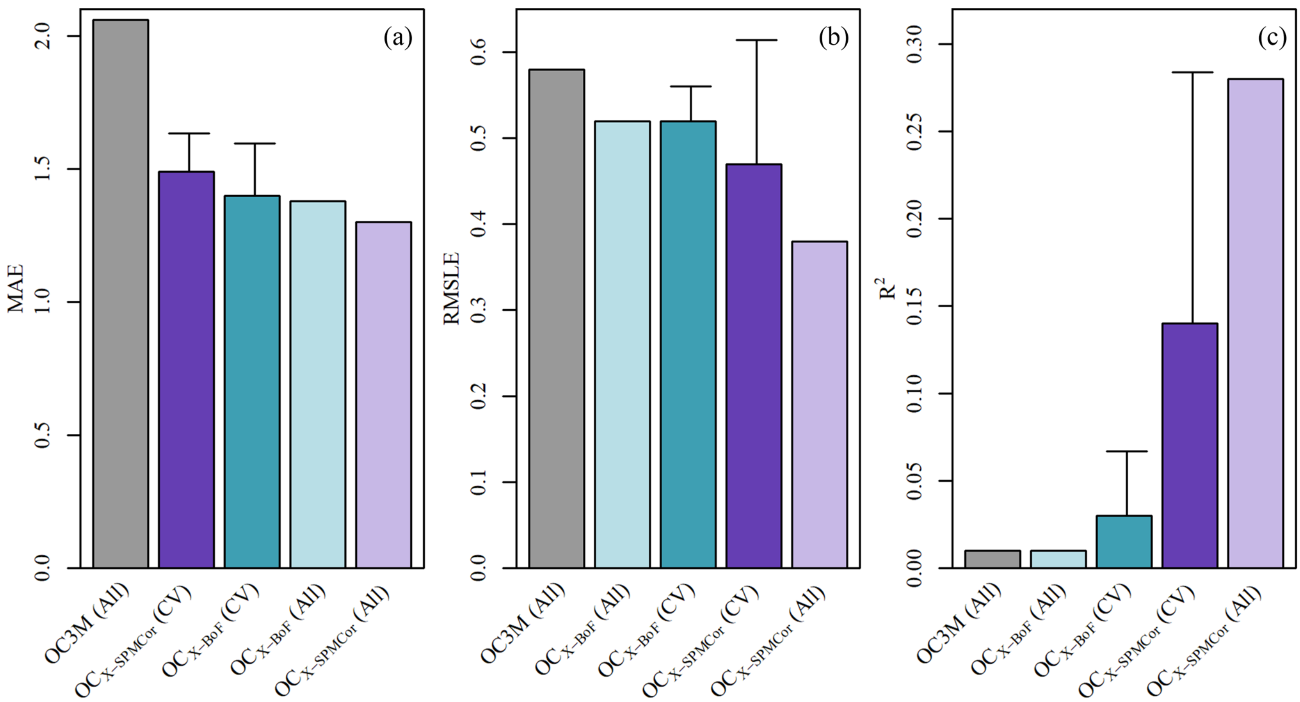

Fig. 5 Mean absolute error (MAE; **a**), root mean square logarithmic error (RMSLE; **b**), and R^2 (**c**) for all data points with the tested chl-a models, and 5-fold cross-validation runs repeated 10 times. Error bars are standard deviation on the cross-validation (CV) runs.

Table 2 Slope, *y*-intercept, and coefficient of determination (R^2) from the linear regression of log-10 transformed satellite-derived chl-a on log-10 transformed in situ chl-a using the Standard Major Axis method of Type 2 regression for OC3M, $OC_{X\text{-BoF}}$, and $OC_{X\text{-SPMCor}}$ with the mean absolute error (MAE), and root mean square logarithmic error (RMSLE) from matchup comparisons. "All" was derived from all in situ data, and cross-validation was averaged following the 5-fold cross-validation runs repeated 10 times where ~34 test samples were used per fold.

	OC3M	$OC_{X\text{-BoF}}$		$OC_{X\text{-SPMCor}}$	
	All	All	Cross-validation	All	Cross-validation
Y-intercept	0.34	0	0.01	0	0.02
Slope	0.80	1	0.37	1	0.50
R^2	0.01	0.01	0.03	0.28	0.14
N	174	174	~34	174	~34
MAE	2.06	1.38	1.40	1.30	1.49
RMSLE	0.58	0.52	0.52	0.38	0.47

and 7b). As only one example, looking closely at a relatively cloud-free image with a single matchup point (Fig. 7), $OC_{X\text{-SPMCor}}$ predicted chl-a of 2.5 mg m^{-3}, only 0.1 mg m^{-3} (4%) higher than the in situ data, relative to the 5.7 mg m^{-3} predicted by OC3M (97% higher). The relationship between SPM and OC3M chl-a had a low positive correlation (R^2 = 0.40) where high chl-a equaled high SPM, while $OC_{X\text{-SPMCor}}$ showed a low negative correlation ($R^2 = -0.42$) where high SPM corresponded to low chl-a (Fig. S4 in Supplementary Materials 4). While only one matchup point was highlighted here, a similar relationship is maintained across all matchup dates. The summer distribution of chl-a peaked in the central bay and decreased in the northeast and southwest (Fig. 7c). While OC3M incorrectly predicted a homogenous spatial distribution of chl-a that increased towards the northeast (Fig. 7a), spatial patterns of chl-a derived from $OC_{X\text{-SPMCor}}$ aligned closely with the in situ data ones (Fig. 7b).

AZMP samples once monthly (weather permitting) a fixed station (Prince 5) within the Bay of Fundy (Fig. 8). At this station, Turner chl-a remained < 1 mg m^{-3} during winter months, increased in spring, and remained elevated all summer ~4 mg m^{-3} (Fig. 8a). The OC3M-derived chl-a monthly climatology did not show a seasonal cycle as chl-a remained at ~4 mg m^{-3} throughout the year (Fig. 8b). This pitfall was addressed when the new $OC_{X\text{-SPMCor}}$ algorithm was used to derive the chl-a monthly climatology with low values in winter (~ 0.5 mg m^{-3}) and high values in summer (up to 5 mg m^{-3}, on average) in agreement with the in situ chl-a seasonal cycle (Fig. 8c). The ability of the $OC_{X\text{-SPMCor}}$ algorithm to capture the seasonal cycle at the annual scale was further demonstrated when examining the entire MODIS time series (2003 to 2021). OC3M data showed little variation with time and systematic overestimation of chl-a compared to the in situ measurements (Fig. 8d), yet there was good agreement between the in situ data and

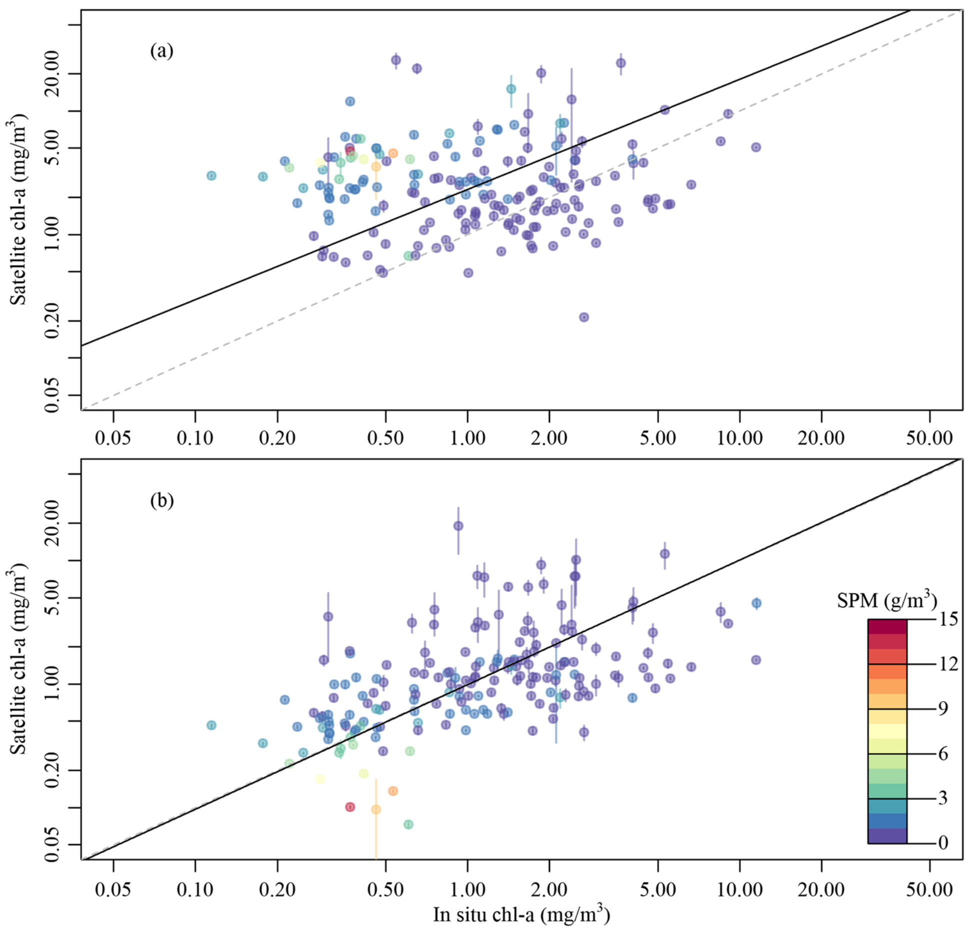

Fig. 6 Satellite matchups based on the standard OC3M algorithm (**a**) and the matchups for the regionally tuned $OC_{X\text{-}SPMCor}$ algorithm (**b**). The grey dashed line corresponds to the 1:1 line and the solid black line corresponds to the regression of in situ versus satellite. Points are colored by the satellite-derived SPM. Vertical lines indicate the median absolute deviation.

the new $OC_{X\text{-}SPMCor}$ chl-a (Fig. 8e). This relationship is best quantified during the spring and summer months. Note that the time series included 41 matchups used in model tuning out of 219 in situ measurements specifically taken at Prince 5. We further validated the algorithm by focusing on two small regions with limited matchup data; see Supplementary Materials 4 for further text and figures.

Annual and Seasonal Climatology

The 2003–2021 chl-a and SPM climatology demonstrated marked spatial distribution within the Bay of Fundy (Fig. 9). Chl-a was highest within Passamaquoddy Bay and around Brier Island, with higher concentrations found in the southwest side of the bay relative to the northeast side. SPM showed an inverse distribution compared to the chl-a one where the highest SPM was observed in Chignecto Bay and Minas Basin, with elevated SPM along the New Brunswick coastline on the western side of the Bay of Fundy. The annual chl-a spatial distribution was driven by the spring and fall climatology which showed the highest chl-a spatial gradients (Fig. 10a, c), while in summer chl-a was highest and most evenly distributed (Fig. 10b). This summer chl-a peak was also observed in the in situ data (Figs. 2, 8, S5, and S6). SPM remained elevated year-round in particular at the head of the Bay of Fundy and along the New Brunswick shore (Fig. 9b). The relative SPM gradients remained in all seasons with the highest SPM observed during winter months (Fig. 11).

Discussion

To understand and quantify the spatial and temporal distribution of chl-a and SPM in the Bay of Fundy, we processed the MODIS time series from 2003 to 2021 onto a 300-m map projection. The tuning of the chl-a algorithm and the addition of an SPM-dependent term significantly improved chl-a retrievals across the Bay of Fundy as shown by comparison against in situ measurements and its ability to resolve the seasonal cycles of chl-a.

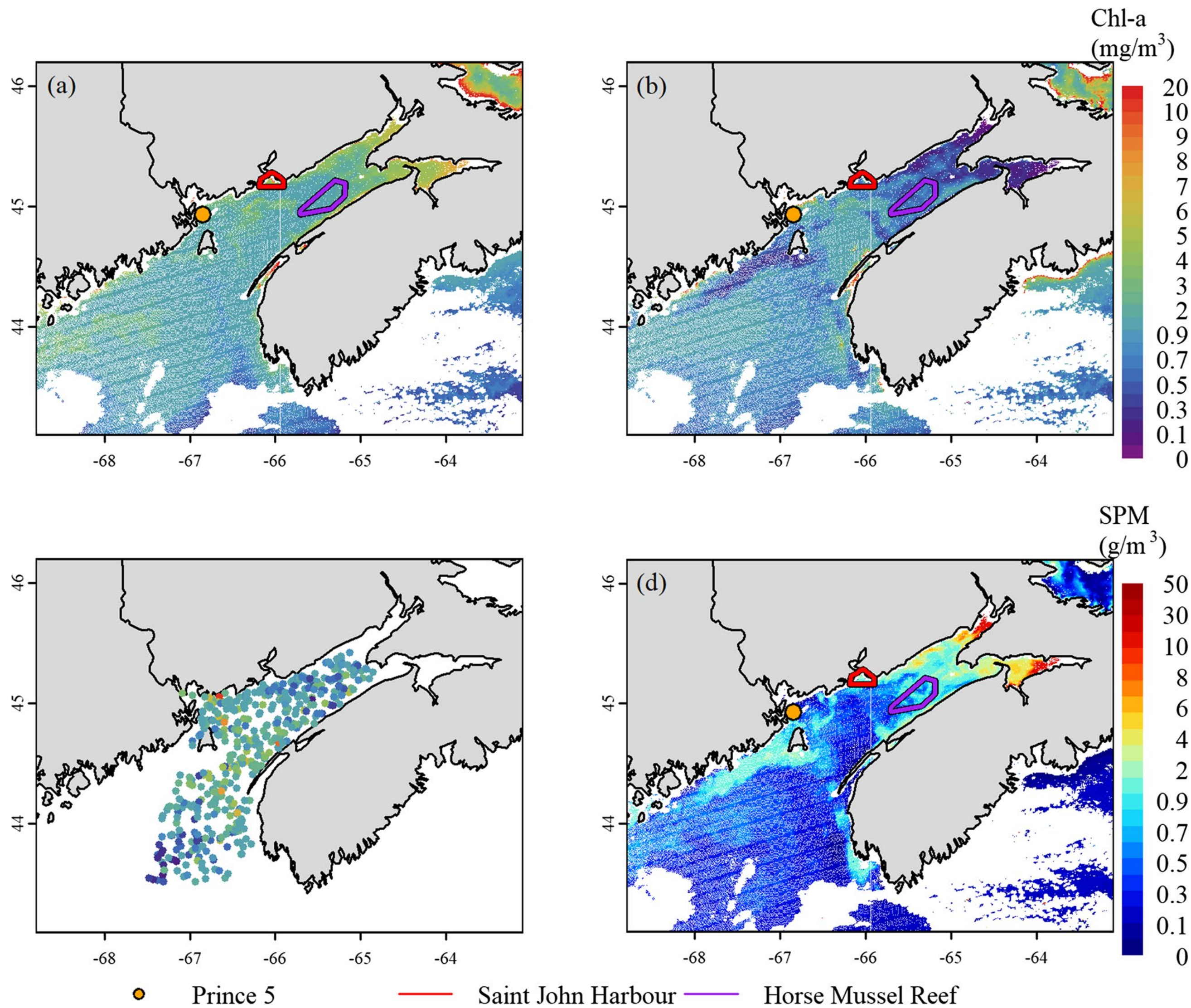

Fig. 7 MODIS daily composite collected on August 12, 2013, showing satellite-derived chl-a using OC3M (**a**), chl-a from $OC_{X\text{-}SPMCor}$ (**b**), all summer in situ Turner chl-a data using the same color scale as **a** and **b** (**c**), and satellite-derived SPM (**d**). The location of the Prince 5 monitoring station, Saint John Harbour, and Horse Mussel Reef Ecologically and Biologically Significant Area (EBSA) are indicated. Moiré patterns are visible in insets **a**, **b**, and **d** as the Bay of Fundy was towards the western edge of the satellite image swath.

SPM Seasonal Cycle and Spatial Distribution

In situ SPM concentrations within the Bay of Fundy are highly variable across season, space, and tidal cycle (Amos and Topliss 1985; Amos and Tee 1989; Schell 1998; Curran et al. 2004; Parker et al. 2007; Zions et al. 2017). We found that while MODIS showed a slight underestimation of SPM using the Nechad algorithm with band 13 (range of 662–672 nm), SPM gradients were well captured across space and time. This underestimation was in part due to the (1) low absolute $R_{rs}(\lambda_{red})$ values that highlight the need for adapted atmospheric correction, and (2) the saturation of the Nechad algorithm for SPM greater than about 50 g m^{-3}. It is noteworthy that while SPM within the Bay of Fundy does exceed 50 g m^{-3}, this typically occurs in the narrow upper reaches of the estuaries where the 300-m spatial resolution, bilinearly interpolated from 500-m and 1-km MODIS bands, is too coarse for SPM mapping. We did not switch to a longer wavelength (e.g., 748 or 869 nm) to derive SPM (Nechad et al. 2010) as the large gradient of SPM requires a wavelength that remains sensitive to low concentrations (< 1 g m^{-3}).

The large variation in SPM in the Minas Basin, even within one tidal cycle (Figs. S1 and S2 in Supplementary Materials 2), makes exact matchup comparisons difficult (Amos and Asprey 1981; Envirosphere Consultants Ltd. 2010; Zions et al. 2017). We explored the use of other red (Han et al. 2016) and green/red-edge bands (Doxaran et al.

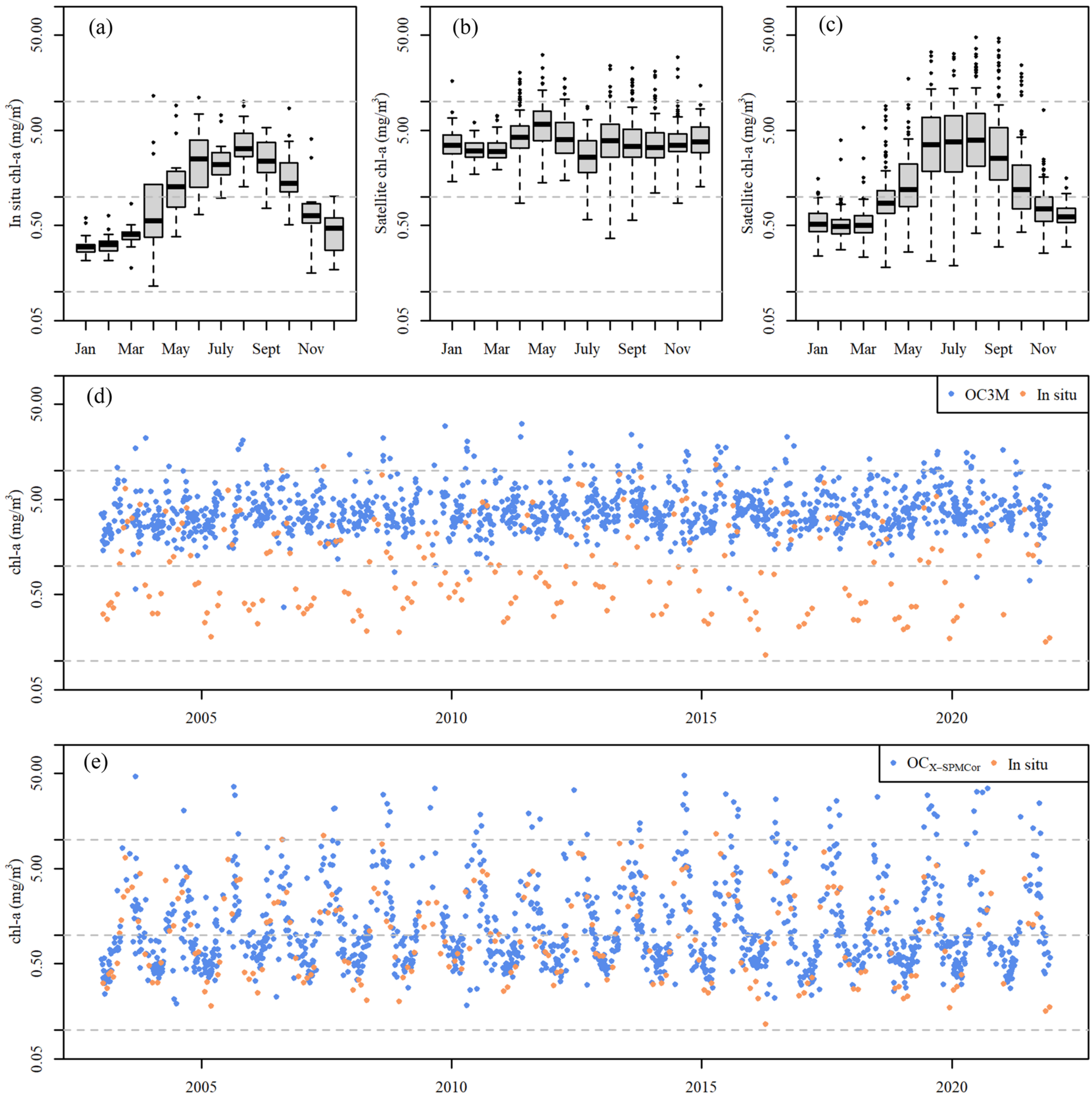

Fig. 8 Monthly in situ Turner chl-a climatology at the Prince 5 monitoring station (**a**), median 5 × 5 box of satellite-derived chl-a calculated with the OC3M algorithm at the station (**b**), and the corresponding median 5 × 5 box of satellite-derived chl-a with the $OC_{X\text{-}SPMCor}$ algorithm (**c**). Time series of satellite-derived chl-a using the OC3M algorithm (**d**) and the $OC_{X\text{-}SPMCor}$ algorithm (**e**) versus in situ data. Note in situ points were from all available data and included data not used in model training.

2012; Doxaran et al. 2015) algorithms for SPM retrieval (results not shown); however, the Nechad algorithm was best at describing the spatial distribution in SPM. Another study in the Minas Basin based on the MEdium Resolution Imaging Spectrometer (MERIS) related the backscattering coefficient at 550 nm to SPM via fixed conversion factors (Tao et al. 2014). The authors then compared the variability of satellite-derived SPM collected in 2010 to in situ measurements collected from 1975 to 1976 for the summer season at the same station. They observed an overall good agreement with a slight underestimation of the magnitude of satellite-derived SPM in summer months from the 2010 satellite data and 1975 to 1976 in situ data, albeit with large standard deviations for both measurements. This study and ours (Fig. 3) demonstrate how the large temporal variation of SPM within the Minas

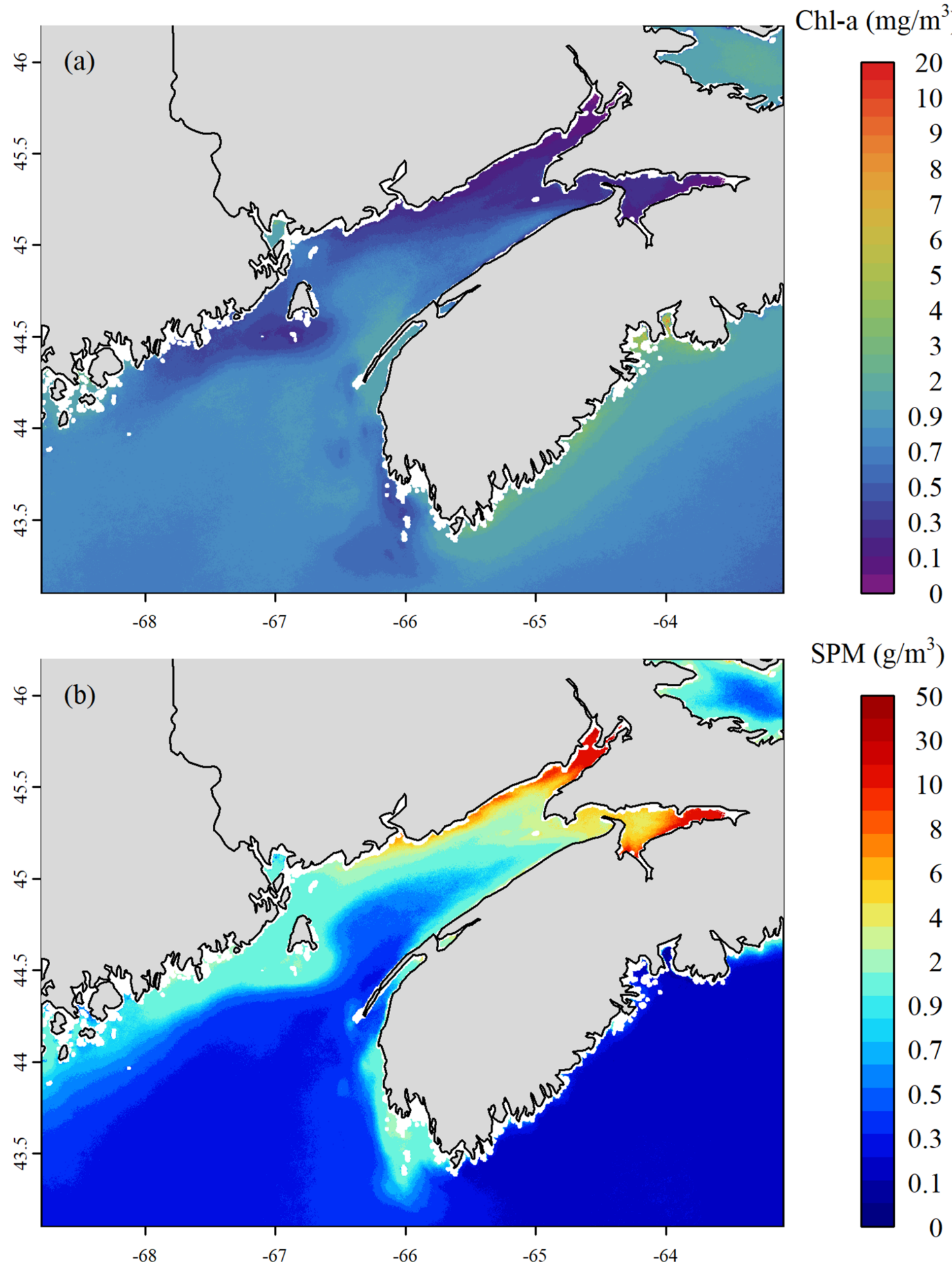

Fig. 9 Annual chl-a derived from the $OC_{X\text{-}SPMCor}$ formula (**a**), and SPM derived from the Nechad algorithm (**b**) climatology from 2003 to 2021.

Basin requires unconventional techniques to validate satellite-derived SPM. For this reason, we chose to look at the relative spatial-temporal trends to validate our SPM retrieval.

SPM peaks in winter and reaches a minimum in summer across the entire Bay of Fundy. The large increase in SPM in winter is driven by increases in wind-induced mixing and wave height which increase sediment resuspension (Mulligan et al. 2019). A previous study from 1980 found that SPM in Chignecto Bay ranged from 36 to 166 g m^{-3} in March with a 80% decrease in mean SPM to between 4 and 42 g m^{-3} in June (Amos and Topliss 1985). The satellite-derived SPM climatology computed in the current study for Chignecto Bay in March ranged from 1 to 25 g m^{-3}, with an average of about 13 g m^{-3}. SPM decreased to 0.2–18 g m^{-3} with a mean SPM of ~5 g m^{-3} by June (60% decrease). In the Minas Basin, SPM also followed a strong seasonal cycle (Tao et al. 2014; Law et al. 2021) with an order of magnitude decrease from March (ranging from 10–100 g m^{-3}) to June (ranging from 1–10 g m^{-3}) (Zions et al. 2017), which was well captured in the MODIS derived SPM maps. When compared to a region with low SPM, historical measurements in October 1990 found Passamaquoddy Bay to be well mixed with surface SPM averaging about 1.8 g m^{-3} (Milligan 1994). This was only 0.3 g m^{-3} higher than the mean October 2003–2021

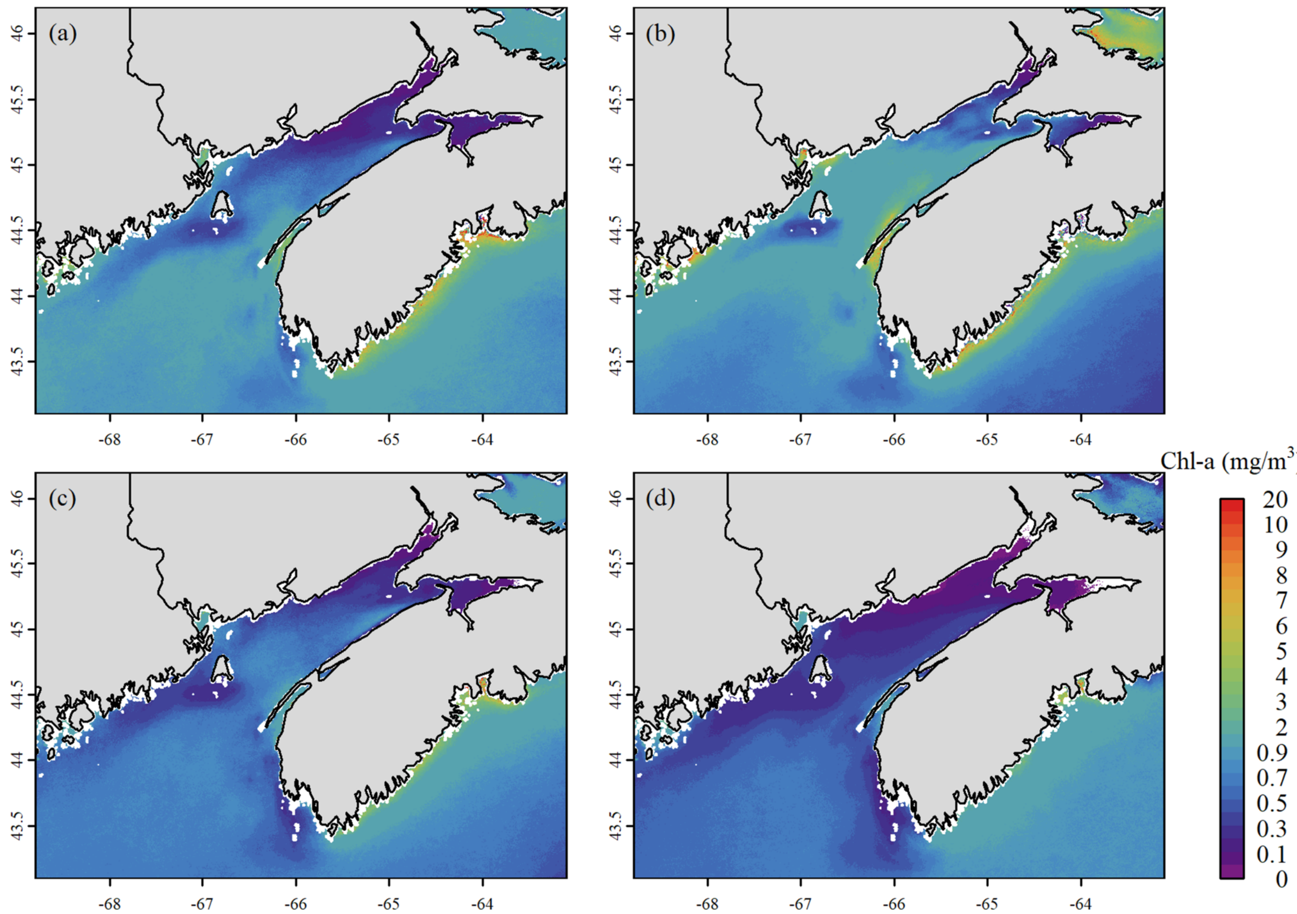

Fig. 10 Chl-a seasonal climatology from 2003 to 2021 for spring (**a** April–June), summer (**b** July–September), fall (**c** October–December), and winter (**d** January–March) based on the $OC_{X\text{-}SPMCor}$ algorithm.

satellite-derived SPM climatology extracted from Passamaquoddy Bay for the same area. Consequently, our MODIS SPM seasonal climatology was able to capture SPM trends across the Bay of Fundy. Furthermore, the seasonal cycle observed within the Bay of Fundy matches the broad-scale SPM dynamics observed along the Scotian Shelf and Northumberland Strait (Swift et al. 1969; Fuentes-Yaco et al. 2020).

SPM reached its maximum in Chignecto Bay and decreased exponentially from NE to SW within the Bay of Fundy. The observed gradient and distribution of SPM are generally consistent with circulation patterns observed in the Bay of Fundy (Swift et al. 1969; Aretxabaleta et al. 2008). Counterclockwise circulation draws waters from the Scotian Shelf and Gulf of Maine northwards along the eastern side of the Bay of Fundy, and tidal forces concentrate sediment-laden waters along the western coast, which remain separated from the Fundy gyre located in the center of the bay (Fader et al. 1977). The decrease in SPM in summer months was particularly noticeable within the central basin, possibly driven by seasonal shifts in the circulation patterns of the Fundy gyre (Aretxabaleta et al. 2008; Aretxabaleta et al. 2009), and the overall reduction in SPM loading within the Chignecto Bay and Minas Basin during the summer when river discharge reaches its minimum.

Chl-a Algorithm

Derivation of reliable chl-a in coastal turbid waters remains challenging and requires regional algorithms that account for the optical complexity of such environments. Several approaches can be used depending on the phytoplankton community structure and the "contamination" of the chl-a signal, namely by CDOM or sediments, which can be characterized as dark waters and bright waters respectively. In the Gulf of Saint Lawrence, Laliberté et al. (2018) and Laliberté and Larouche (2023) used an empirical orthogonal functions (EOF) method to infer satellite-based chl-a from R_{rs} in waters dominated by CDOM absorption. The red-edge method performs best in meso- to eutrophic environments where chl-a exceeds 10 mg m^{-3} (Dall'Olmo et al. 2005; Maciel et al. 2023), such that its range of application

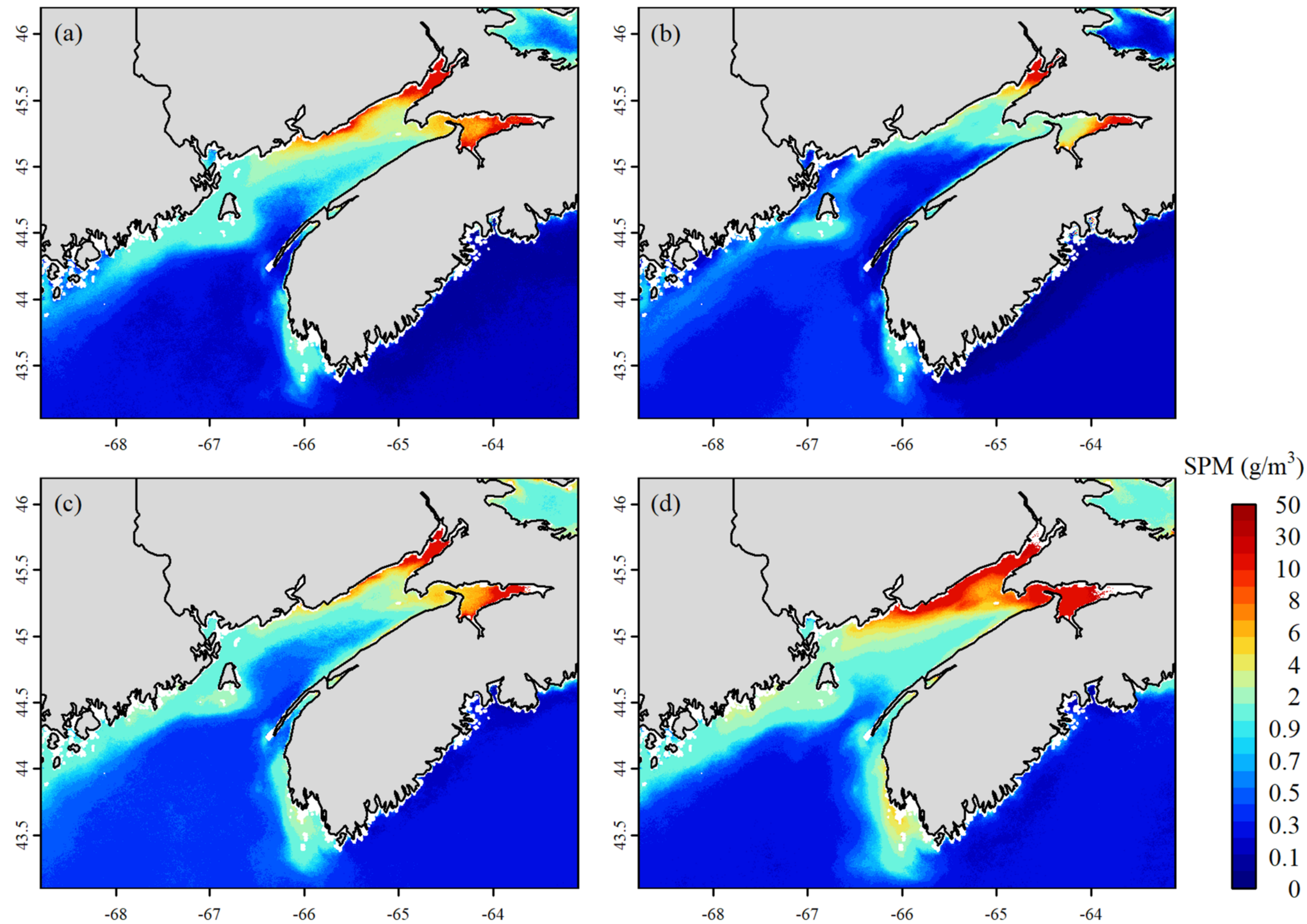

Fig. 11 SPM seasonal climatology from 2003 to 2021 for spring (**a** April–June), summer (**b** July–September), fall (**c** October–December), and winter (**d** January–March) based on the Nechad algorithm.

is not suitable to the Bay of Fundy where chl-a is less than 5 mg m^{-3} for most of the year (Fig. 2). The fluorescence line height proposed by Gower et al. (1990) was also considered; however, issues related to phytoplankton sun-induced-fluorescence peak shift in sediment-loaded waters precluded the use of this algorithm. In addition, other issues related to spectral resolution, required to characterize the fluorescence peak, phytoplankton physiological status, and impact of the inherent optical properties budgets on the fluorescence emission remain unresolved (Gupana et al. 2021).

Given the physical characteristics of the Bay of Fundy, namely productive waters in a sediment-loaded environment, we selected an adapted atmospheric correction scheme (NIR-SWIR switching algorithm; Wang and Shi 2007). The NIR-SWIR returned the lowest number of negative R_{rs} when considering the wavelengths in the visible spectrum based on comparison with other procedures (results now shown) such as black pixel assumption (Siegel et al. 2000) and MUMM approach (Ruddick et al. 2006). A simple approach was chosen to retrieve chl-a that still relied on a blue-green band ratio, but with an additional term that corrected for the possible contamination of the chl-a signal by the bright SPM signal. The estimation of the chl-a relied on the usual blue-green ratio and the additional term that accounted for possible contamination by SPM relied on the red band (i.e., 670 nm). Two different red terms were tested; first was the $R_{rs}(\lambda_{670})$ values, second was the SPM values calculated from this same band. The use of the SPM values provided slightly better results than the $R_{rs}(\lambda_{670})$ ones (results not shown here), suggesting that highly non-linear processes occur in the coupling of chl-a/SPM signal. The regional tuning of the final $OC_{X\text{-}SPMCor}$ algorithm saw slight modification of the two first coefficients of the polynomial fit (Eq. 4) with values of $a_0 = 0.24$ and $a_1 = -2.74$ for OC3M and $a_0 = -0.23$ and $a_1 = -2.81$ for $OC_{X\text{-}SPMCor}$; however, the subsequent coefficients (second and higher polynomial order) were very different between both parameterizations. The polynomial coefficient associated with SPM is negative, which was expected as the inclusion of SPM in the new formulation reduced the overestimation of chl-a observed with

OC3M. Interestingly, the SPM algorithm is based on the 670 nm band, which corresponds to the second absorption peak of chl-a such that there is an interplay between SPM and chl-a in the algorithm. Yet, as the coefficients for $OC_{X\text{-}SPMCor}$ were locally tuned, the correlation between chl-a and SPM at 670 nm would be embedded in the algorithm. Furthermore, in a low SPM environment, there would be a negligible impact of SPM on the $OC_{X\text{-}SPMCor}$ algorithm. Future studies could explore potential switching thresholds as done in other SPM algorithms (Han et al. 2016), but applied to the $OC_{X\text{-}SPMCor}$ algorithm to reduce or remove the SPM term in chl-a retrieval at low SPM. The bi-modal distribution of the a_0 term for $OC_{X\text{-}SPMCor}$ (Supplementary Materials 3) was driven by SPM concentration, where high SPM (≥ 1 g m^{-3}) pushed a_0 to a lower value and low SPM (< 1 g m^{-3}) drove a_0 to a higher value (results not shown). This suggests that further improvements in chl-a retrieval may be possible if tuning was performed for these two groups separately, and blended into a single algorithm. Finally, we opted to train the $OC_{X\text{-}SPMCor}$ model using all available in situ points due to the small number of matchups ($n = 174$), and the even smaller number of matchups at high SPM. The poor performance of some cross-validation runs highlighted the importance that a few points may have on the model performance, in particular at high SPM. This demonstrated the need for the largest number of training points possible for the development of $OC_{X\text{-}SPMCor}$; it also suggested that the stability of model coefficients may improve with additional matchups. Regardless, $OC_{X\text{-}SPMCor}$ outperformed all other models tested in the Bay of Fundy.

Past remote sensing studies have attempted to predict chl-a in the Bay of Fundy using generic OCx algorithms. Devred et al. (2018) produced a chl-a climatology from 1998 to 2007 using the OC4 algorithm dedicated to the Sea-viewing Wide Field-of-view Sensor (SeaWiFS) to develop a warning system for the harmful algae *Alexandrium catenella sp*. The OC4 algorithm benefits from an additional band (510 nm) from the SeaWiFS sensor (O'Reilly et al. 1998) and the chl-a climatology indicated a spring/fall bloom sequence (Devred et al. 2018) as opposed to the spring/summer peak revealed by in situ measurements. A MODIS climatology from 2003 to 2012 created for the Gulf of Maine, including the Bay of Fundy and Scotian Shelf with a gap-filling algorithm (Li and He 2014), revealed elevated chl-a year-round in the Bay of Fundy relative to the Gulf of Maine and Scotian Shelf. Yet, satellite-derived chl-a was validated using in situ data collected on the Scotian Shelf, which is known to have a different chl-a phenology and SPM regime than the Bay of Fundy (Casault et al. 2023). Our study highlights the importance of regional tuning for chl-a retrieval within the Bay of Fundy, which is impacted by high sediment loads, strong tidal forces, and shows a different chl-a phenology than surrounding waters. Such recalibration of global algorithms has been commonly performed to improve chl-a retrieval in the complex waters of the Northwest Atlantic (Laliberté et al. 2018; Clay et al. 2019).

A limitation of the regional $OC_{X\text{-}SPMCor}$ algorithm was the limited range of SPM at which it was tuned. $OC_{X\text{-}SPMCor}$ was parameterized for SPM < 15 g m^{-3} with most pixels corresponding to SPM < 5 g m^{-3}, which resulted in an overcorrection (i.e., underestimation) of chl-a at SPM > 5 g m^{-3}. For instance, in Chignecto Bay, historical chl-a data averaged 1.3–1.8 mg m^{-3} with no seasonal variation (Prouse et al. 1984), while the $OC_{X\text{-}SPMCor}$ derived chl-a climatology predicted a much lower chl-a average of ~0.2 mg m^{-3}; the seasonal climatology correctly predicted the low seasonal variation. We did not have access to chl-a collected at high temporal frequency (i.e., multiple times a day), as we did for the SPM data. Given the large diurnal variation in SPM, it is likely that chl-a exhibits a diurnal variation, and restricting chl-a matchups to within a few hours of water sample collection may improve our matchup statistics. Our validation was further limited to the Bay of Fundy and no validation of the algorithm was performed for the Gulf of Maine, Scotian Shelf, or Northumberland Strait, which were not in the scope of the present study. Future work will examine how to blend the Bay of Fundy specific regional algorithm ($OC_{X\text{-}SPMCor}$) into larger areas of the Northwest Atlantic, such as the Gulf of Maine and Scotian Shelf, where other regional chl-a models already exist and perform well (Clay et al. 2019). Lastly, our regional calibration was performed using Turner chl-a due to its better spatial and temporal coverage across the Bay of Fundy than HPLC-based chl-a. While HPLC is recommended for chl-a algorithm development, Turner-derived chl-a is more ubiquitous as analysis of samples is much easier, requires less technical skill than HPLC-based measurements, and has been used for satellite validation in other studies (Cannizzaro et al. 2013; Brewin et al. 2017; Laliberté et al. 2018). Our study highlights that significant improvements in chl-a retrieval can be obtained with only Turner chl-a, which had a much better temporal and spatial availability relative to HPLC samples.

Chl-a Seasonal Cycle and Spatial Distribution

Chl-a within the Bay of Fundy followed a consistent seasonal cycle, which was opposite to SPM as revealed by both satellite and in situ measurements. When chl-a was calculated with the OC3M algorithm, this relationship was not maintained, and chl-a was calculated to increase with SPM. In particular, chl-a retrieval was more significantly impacted at SPM > 1 g m^{-3}. Tuning the algorithm for the Bay of Fundy and including an SPM term improved the $OC_{X\text{-}SPMCor}$ algorithm chl-a retrieval and its relationship to SPM, where chl-a typically peaked in late summer and reached a minimum in winter, and SPM peaked in winter and reached a minimum in summer.

To highlight our improvements in chl-a retrieval, we focused on three distinct regions of the Bay of Fundy and demonstrated improved satellite results when compared to in situ data. The first, Prince 5 is located at the entrance of the highly productive Passamaquoddy Bay, which has been designated as an EBSA (Buzeta 2014), and is sampled monthly by AZMP (Casault et al. 2023). This station has the best temporal coverage of in situ chl-a with samples across all months, and a clear seasonal cycle as revealed by a spring bloom and a second summer peak in chl-a. The initial OC3M algorithm generated a time series of elevated chl-a throughout the year with no seasonal variation, as found in other satellite remote sensing studies (Li and He 2014; Fuentes-Yaco et al. 2020). The new $OC_{X\text{-}SPMCor}$ closely followed the seasonal cycle and magnitude of in situ data. The EBSA, Horse Mussel Reef (Buzeta 2014), located in the center of the Bay of Fundy showed lower chl-a and a reduced seasonal cycle compared to Prince 5. Lastly, Saint John Harbour, a region that is strongly impacted by the tidal cycle and outputs from the Saint John River, showed a comparable chl-a seasonal pattern to Prince 5, albeit at lower concentrations.

Chl-a seasonality for these three regions, and for the Bay of Fundy as a whole, followed a particular annual cycle that differs from the adjacent Scotian Shelf which has marked spring and fall blooms (Casault et al. 2023). Instead, the seasonal cycle of phytoplankton was correlated to changes in day length (Percy et al. 1996), and after a rapid increase in spring, chl-a remained elevated all summer. Furthermore, these periods of high chl-a (spring and summer), corresponded to increased stratification within the Fundy gyre (Aretxabaleta et al. 2008; Aretxabaleta et al. 2009). Yet, significant tidal mixing occurs within the shallow waters of the bay with further interactions of the Saint John River discharge during spring months. This strong and variable tidal mixing, and influence of river discharge as observed at Prince 5, west of the gyre (Casault et al. 2023), may contribute to persistently high spring and summer chl-a values within the Bay of Fundy by providing a continuous supply of nutrients to the central bay. Our description of chl-a phenology in the Bay of Fundy would be further improved if additional in situ chl-a samples were collected in the upper reaches of the bay where the highest sediment concentrations occur.

Summary and Conclusions

The Bay of Fundy is a unique environment subjected to the highest tidal range in the world with inputs from several rivers. This results in large temporal and spatial variability in SPM and chl-a and seasonal cycles that differ from the adjacent Gulf of Maine and Scotian Shelf. The optical complexity of the Bay of Fundy required the tuning of the OC3M satellite chl-a band ratio algorithm and in particular, the addition of a SPM-dependent term in the mathematical formulation of the algorithm to correct for systematic bias. This tuning, validated with a large database of in situ Turner chl-a measurements, significantly improved the performance of the algorithm and provided the ability to resolve the seasonal cycle of chl-a in all the regions of the Bay of Fundy under different SPM regimes.

The 2003–2021 SPM climatology provided the general distribution and spatial gradients of SPM, which decreased exponentially from northeast to southwest, and remain elevated along the New Brunswick coast, as expected by circulation patterns within the Bay of Fundy. SPM peaks in winter when turbulent mixing is the highest and reaches a minimum in the summer months. The new $OC_{X\text{-}SPMCor}$ algorithm accurately predicted the unique chl-a phenology within the Bay of Fundy, relative to the surrounding regions. In the Bay of Fundy, chl-a blooms in spring, and remains high all summer, before reaching a winter minimum. The exception to this phenology were in the upper reaches of the Bay of Fundy where chl-a shows little seasonal fluctuation. Our study is the first to quantify chl-a and SPM dynamics specifically for the entire Bay of Fundy with reliable, and validated satellite observation. It highlights the importance of considering the effects of varying sediment dynamics on chl-a retrieval within these optically complex waters.

Supplementary Information The online version contains supplementary material available at https://doi.org/10.1007/s12237-024-01334-x.

Acknowledgements We thank Benoit Casault and Brendan DeTracey for providing feedback on the manuscript. We also thank the NASA Ocean Biology Processing Group for providing open access to the MODIS-Aqua data, as well as making the SeaDAS processing software available. Further thanks to the creators and maintainers of GMT. Finally, we would like to acknowledge the work of many scientists and technicians for collecting, analyzing, and documenting the large volume of in situ samples used in this study.

Funding Open access funding provided by Fisheries & Oceans Canada library. Fisheries and Oceans Canada Marine Conservation Targets.

Data Availability MODIS-Aqua data is available at https://oceancolor.gsfc.nasa.gov/. All code used in this analysis is available on the following GitHub repository: https://github.com/BIO-RSG/Improving-satellite-chlorophyll-a-retrieval-in-the-turbid-waters-of-the-Bay-of-Fundy-Canada.git. Ocean color processing algorithms and functions mentioned in the text were made available in the “oceancolouR” package (https://github.com/BIO-RSG/oceancolouR). Seasonal and annual chl-a and SPM geotiff layers are hosted on the Government of Canada’s Open Data (https://open.canada.ca/data/en/dataset/272f5cf1-52bb-416b-b92a-8bc9384fc24d). Daily chl-a and SPM composites will be provided upon request.

Declarations

Conflict of Interest The authors declare no competing interests.

References

Amos, C.L., and T.T. Alfoldi. 1979. The determination of suspended sediment concentration in a macrotidal system using Landsat data. *Journal of Sedimentary Research* 49: 0159–0174. https://doi.org/10.1306/212f76df-2b24-11d7-8648000102c1865d.

Amos, C. L., and K. W. Asprey. 1981. An interpretation of oceanographic and sediment data from the upper Bay of Fundy. *Report Series* BI-R-81-15: vii + 143 p.

Amos, C. L., and B. F. N. Long. 1980. The sedimentary character of the Minas Basin, Bay of Fundy. *The Coastline of Canada, Littoral Processes and Shore Morphology - Proceedings of a Conference Held in Halifax, May 1-3, 1978*.

Amos, C.L., and K.T. Tee. 1989. Suspended sediment transport processes in Cumberland Basin, Bay of Fundy. *Journal of Geophysical Research* 94: 407–417. https://doi.org/10.1029/jc094ic10p14407.

Amos, C.L., and B.J. Topliss. 1985. Discrimination of suspended particulate matter in the Bay of Fundy using the Nimbus 7 Coastal Zone Color Scanner. *Canadian Journal of Remote Sensing* 11: 85–92. https://doi.org/10.1080/07038992.1985.10855080.

Aretxabaleta, A.L., D.J. McGillicuddy, K.W. Smith, and D.R. Lynch. 2008. Model simulations of the Bay of Fundy Gyre: 1. Climatological results. *Journal of Geophysical Research: Oceans* 113: C9. https://doi.org/10.1029/2007JC004480.

Aretxabaleta, A.L., D.J. McGillicuddy, K.W. Smith, J.P. Manning, and D.R. Lynch. 2009. Model simulations of the Bay of Fundy gyre: 2. Hindcasts for 2005–2007 reveal interannual variability in retentiveness. *Journal of Geophysical Research: Oceans* 114: C10. https://doi.org/10.1029/2008JC004948.

Ashall, L. M., R. P. Mulligan, and B. A. Law. 2016. Variability in suspended sediment concentration in the Minas Basin, Bay of Fundy, and implications for changes due to tidal power extraction. *Coastal Engineering* 107: 102–115. https://doi.org/10.1016/j.coastaleng.2015.10.003.

Brewin, R. J. W., S. Ciavatta, S. Sathyendranath, T. Jackson, G. Tilstone, K. Curran, R. L. Airs, et al. 2017. Uncertainty in ocean-color estimates of chlorophyll for phytoplankton groups. *Frontiers in Marine Science* 4: 104. https://doi.org/10.3389/fmars.2017.00104.

Buzeta, M.-I. 2014. Identification and review of ecologically and biologically significant areas in the Bay of Fundy. *Canadian Science Advisory Secretariat Research Documents* 2013/065: vi + 59 p.

Camiolo, M.D., E. Cozzolino, A.I. Dogliotti, C.G. Simionato, and C.A. Lasta. 2019. An empirical remote sensing algorithm for retrieving total suspended matter in a large estuarine region. *Scientia Marina* 83: 53–60. https://doi.org/10.3989/scimar.04847.22A.

Cannizzaro, J.P., C. Hu, K.L. Carder, C.R. Kelble, N. Melo, E.M. Johns, C.A. Vargo, and G.A., and Heil. 2013. On the accuracy of SeaWiFS ocean color data products on the West Florida shelf. *Journal of Coastal Research* 29: 1257. https://doi.org/10.2112/JCOASTRES-D-12-00223.1.

Canty, A., and B. D. Ripley. 2022. boot: bootstrap functions. R package version 1.3-28.1. https://cran.r-project.org/web/packages/boot/.

Casault, B., C. L. Johnson, E. Devred, and L. I. Beazley. 2023. Optical, chemical, and biological oceanographic conditions on the Scotian Shelf and in the eastern Gulf of Maine during 2021. *DFO Canadian Science Advisory Secretariat Research Documents* 2023/016: v + 74 p. https://doi.org/10.13140/RG.2.2.29074.43205.

Clay, S., A. Peña, B. DeTracey, and E. Devred. 2019. Evaluation of satellite-based algorithms to retrieve chlorophyll-a concentration in the Canadian Atlantic and Pacific Oceans. *Remote Sensing* 11: 2609. https://doi.org/10.3390/rs11222609.

Curran, K. J., T. G. Milligan, G. Bugden, B. A. Law, and M. Scotney. 2004. Suspended sediment, water quality, and hydrodynamics of the Petitcodiac River Estuary, New Brunswick (2002 – 2003). *Canadian Technical Report of Fisheries and Aquatic Sciences* 2516: xi + 88 p.

Dall'Olmo, G., A. A. Gitelson, D. C. Rundquist, B. Leavitt, T. Barrow, and J. C. Holz. 2005. Assessing the potential of SeaWiFS and MODIS for estimating chlorophyll concentration in turbid productive waters using red and near-infrared bands. *Remote Sensing of Environment* 96: 176–187. https://doi.org/10.1016/j.rse.2005.02.007.

Dalrymple, R.W., R.J. Knight, B.A. Zaitlin, and G.V. Middleton. 1990. Dynamics and facies model of a macrotidal sand-bar complex, Cobequid Bay—Salmon River Estuary (Bay of Fundy). *Sedimentology* 37: 577–612. https://doi.org/10.1111/j.1365-3091.1990.tb00624.x.

Davison, A., and D. Hinkley. 1997. *Bootstrap methods and their applications*. Cambridge, UK: Cambridge University Press.

Devine, L., M. K. Kennedy, I. St-Pierre, C. Lafleur, M. Ouellet, and S. Bond. 2014. BioChem: the Fisheries and Oceans Canada database for biological and chemical data. *Canadian Technical Report of Fisheries and Aquatic Sciences* 3073: iv + 40 p.

Devred, E., J. Martin, S. Sathyendranath, V. Stuart, E. Horne, T. Platt, M.H. Forget, and P. Smith. 2018. Development of a conceptual warning system for toxic levels of *Alexandrium fundyense* in the Bay of Fundy based on remote sensing data. *Remote Sensing of Environment* 211: 413–424. https://doi.org/10.1016/j.rse.2018.04.022.

Dogliotti, A. I., J. I. Gossn, C. Gonzalez, L. Yema, M. L. Sanchez, and I. O'Farrell. 2021. Evaluation of multi- and hyper-spectral chl-a algorithms in the Río De La Plata turbid waters during a cyanobacteria bloom. *International Geoscience and Remote Sensing Symposium (IGARSS)*: 7442–7445. https://doi.org/10.1109/IGARSS47720.2021.9553148.

Doxaran, D., E. Devred, and M. Babin. 2015. A 50 % increase in the mass of terrestrial particles delivered by the Mackenzie River into the Beaufort Sea (Canadian Arctic Ocean) over the last 10 years. *Biogeosciences* 12: 3551–3565. https://doi.org/10.5194/bg-12-3551-2015.

Doxaran, D., J. Ehn, S. Bélanger, A. Matsuoka, S. Hooker, and M. Babin. 2012. Optical characterisation of suspended particles in the Mackenzie River plume (Canadian Arctic Ocean) and implications for ocean colour remote sensing. *Biogeosciences* 9: 3213–3229. https://doi.org/10.5194/bg-9-3213-2012.

Envirosphere Consultants Ltd. 2010. Oceanographic measurements — salinity, temperature, suspended sediment & turbidity, Minas Passage Study Site June - August 2009.

Fader, G. B., L. H. King, and B. MacLean. 1977. Surficial geology of the eastern Gulf of Maine and Bay of Fundy. *Geological Survey of Canada Paper.* 76–17: iv + 1-23 p.

Franz, B. A., P. J. Werdell, G. Meister, E. J. Kwiatkowska, S. W. Bailey, Z. Ahmad, and C. R. McClain. 2006. MODIS land bands for ocean remote sensing applications. In *Proc. Ocean Optics XVIII, Montreal, Canada, 9-13 October 2006*.

Fuentes-Yaco, C., S. Parsons, M. Hardy, S. Clay, E. Horne, B. A. Law, C. Caverhill, et al. 2020. The importance of including satellite remotely-sensed ocean colour analyses to the planning of airborne lidar bathymetry. *Canadian Technical Report of Fisheries and Aquatic Sciences* 3366: xli + 299 p.

Garrett, C. 1972. Tidal resonance in the Bay of Fundy and Gulf of Maine. *Nature* 238: 441–443. https://doi.org/10.1038/238441a0.

Gower, J.F.R., and G.A. Borstad. 1990. Mapping of phytoplankton by solar-stimulated fluorescence using an imaging spectrometer. *International Journal of Remote Sensing* 11: 313–320. https://doi.org/10.1080/01431169008955022.

Greenberg, D.A., and C.L. Amos. 1983. Suspended sediment transport and deposition modeling in the Bay of Fundy, Nova Scotia — a region of potential tidal power development. *Canadian Journal of Fisheries and Aquatic Sciences* 40: 20–34. https://doi.org/10.1139/f83-266.

Gupana, R. S., D. Odermatt, I. Cesana, C. Giardino, L. Nedbal, and A. Damm. 2021. Remote sensing of sun-induced chlorophyll-a fluorescence in inland and coastal waters: current state and future prospects. *Remote Sensing of Environment* 262: 112482. https://doi.org/10.1016/j.rse.2021.112482.

Hamner, B., M. Frasco, and E. LeDell. 2022. Metrics: evaluation metrics for machine learning. R package version 0.1.4. https://cran.r-project.org/web/packages/Metrics/.

Han, B., H. Loisel, V. Vantrepotte, X. Mériaux, P. Bryère, S. Ouillon, D. Dessailly, Q. Xing, and J. Zhu. 2016. Development of a semi-analytical algorithm for the retrieval of suspended particulate matter from remote sensing over clear to very turbid waters. *Remote Sensing* 8: 211. https://doi.org/10.3390/rs8030211.

Hilborn, A., and E. Devred. 2022. Delineation of Eastern Beaufort Sea sub-regions using Self-Organizing Maps applied to 17 years of MODIS-Aqua data. *Frontiers in Marine Science* 9: 912865. https://doi.org/10.3389/fmars.2022.912865.

Holm-Hansen, O., C.J. Lorenzen, R.W. Holmes, and J.D.H. Strickland. 1965. Fluorometric determination of chlorophyll. *ICES Journal of Marine Science* 30: 3–15. https://doi.org/10.1093/icesjms/30.1.3.

Horne, E., and B. A. Law. 2013. *Cruise report Hudson 2013013 Minas Basin June 4 - 16, 2013*.

Hu, C., Z. Lee, and B. Franz. 2012. Chlorophyll a algorithms for oligotrophic oceans: a novel approach based on three-band reflectance difference. *Journal of Geophysical Research: Oceans* 117: C01011. https://doi.org/10.1029/2011JC007395.

Laliberté, J., and P. Larouche. 2023. Chlorophyll-a concentration climatology, phenology, and trends in the optically complex waters of the St. Lawrence Estuary and Gulf. *Journal of Marine Systems* 238: 103830. https://doi.org/10.1016/j.jmarsys.2022.103830.

Laliberté, J., P. Larouche, E. Devred, and S. Craig. 2018. Chlorophyll-a concentration retrieval in the optically complex waters of the St. Lawrence Estuary and Gulf using principal component analysis. *Remote Sensing* 10: 265. https://doi.org/10.3390/rs10020265.

Law, B.A., T.G. Milligan, P.S. Hill, and G.L. Bugden. 2021. The effect of concentration on particle settling in the Minas Basin. *Nova Scotia. Continental Shelf Research* 223: 104448. https://doi.org/10.1016/j.csr.2021.104448.

Legendre, P. 2022. Lmodel2: model II regression. R Package Version 1.7-3. https://cran.r-project.org/web/packages/lmodel2/.

Lewis, K. M., and K. R. Arrigo. 2020. Ocean color algorithms for estimating chlorophyll a, CDOM absorption, and particle backscattering in the Arctic Ocean. *Journal of Geophysical Research: Oceans* 125: e2019JC015706. https://doi.org/10.1029/2019JC015706.

Li, Y., and R. He. 2014. Spatial and temporal variability of SST and ocean color in the Gulf of Maine based on cloud-free SST and chlorophyll reconstructions in 2003-2012. *Remote Sensing of Environment* 144: 98–108. https://doi.org/10.1016/j.rse.2014.01.019.

Maciel, F. P., S. Haakonsson, L. Ponce de León, S. Bonilla, and F. Pedocchi. 2023. Challenges for chlorophyll-a remote sensing in a highly variable turbidity estuary, an implementation with Sentinel-2. *Geocarto International* 38: 2160017. https://doi.org/10.1080/10106049.2022.2160017.

Martin, J. L., M. M. Legresley, and M. E. Gidney. 2014. Phytoplankton monitoring in the Western Isles region of the Bay of Fundy during 2007-2013. *Canadian Technical Report of Fisheries and Aquatic Sciences* 3105: v + 262 p.

McLeod, E., G.L. Chmura, S. Bouillon, R. Salm, M. Björk, C.M. Duarte, C.E. Lovelock, W.H. Schlesinger, and B.R. Silliman. 2011. A blueprint for blue carbon: toward an improved understanding of the role of vegetated coastal habitats in sequestering CO_2. *Frontiers in Ecology and the Environment* 9: 552–560. https://doi.org/10.1890/110004.

Milligan, T. G. 1994. Suspended and bottom sediment grain size distribution in Letand Inlet, NS., October 1990. *Canadian Technical Report of Hydrography and Ocean Sciences* 156: iv + 51 p.

Minello, T.J., K.W. Able, M.P. Weinstein, and C.G. Hays. 2003. Salt marshes as nurseries for nekton: testing hypotheses on density, growth and survival through meta-analysis. *Marine Ecology Progress Series* 246: 39–59. https://doi.org/10.3354/meps246039.

Mitchell, M. R., G. Harrison, K. Paule, A. Gagné, G. Maillet, and P. Strain. 2002. Atlantic Zonal Monitoring Program sampling protocol. *Canadian Technical Report of Fisheries and Aquatic Sciences* 223: iv + 23 p.

Möller, I., M. Kudella, F. Rupprecht, T. Spencer, M. Paul, B.K. Van Wesenbeeck, G. Wolters, et al. 2014. Wave attenuation over coastal salt marshes under storm surge conditions. *Nature Geoscience* 7: 727–731. https://doi.org/10.1038/NGEO2251.

Mulligan, R. P., P. C. Smith, J. Tao, and P. S. Hill. 2019. Wind-wave and tidally driven sediment resuspension in a macrotidal basin. *Estuaries and Coasts* 42: 641–654. https://doi.org/10.1007/s12237-018-00511-z.

Nechad, B., K.G. Ruddick, and Y. Park. 2010. Calibration and validation of a generic multisensor algorithm for mapping of total suspended matter in turbid waters. *Remote Sensing of Environment* 114: 854–866. https://doi.org/10.1016/j.rse.2009.11.022.

O'Reilly, J.E., S. Maritorena, B.G. Mitchell, D.A. Siegel, K.L. Carder, S.A. Garver, M. Kahru, and C. McClain. 1998. Ocean color chlorophyll algorithms for SeaWiFS. *Journal of Geophysical Research: Oceans* 103: 24937–24953. https://doi.org/10.1029/98JC02160.

Oceans and Coastal Management Division Fisheries and Oceans Canada. 2017. *Musquash estuary a management plan for the marine protected area and administered intertidal area*. Dartmouth, Nova Scotia.

Ody, A., D. Doxaran, Q. Vanhellemont, B. Nechad, S. Novoa, G. Many, F. Bourrin, R. Verney, I. Pairaud, and B. Gentili. 2016. Potential of high spatial and temporal ocean color satellite data to study the dynamics of suspended particles in a micro-tidal river plume. *Remote Sensing* 8: 245. https://doi.org/10.3390/rs8030245.

Parker, M., M. Westhead, and A. Service. 2007. Ecosystem overview report for the Minas Basin, Nova Scotia. *Fisheries and Oceans Canada. Oceans and Habitat Report* 05: xvi + 179 p.

Percy, J., P. Wells, A. J. Evans, and (eds). 1996. Bay of Fundy Issues: a scientific overview. Workshop Proceedings, Wolfville, NS., January 29 to February 1, 1996. Environment Canada - Atlantic

Region Occasional Report no. 8, Environment Canada, Sackville, New Brunswick, 191 pp.

Prouse, N., D.C. Gordon Jr., B.T. Hargrave, C.J. Bird, J. McLachlan, J.S. Lakshminarayana, J. Sita Devi, and M.L.H. Thomas. 1984. Primary production: organic matter supply to ecosystems in the Bay of Fundy. *Canadian Technical Report of Fisheries and Aquatic Sciences* 1236: 65–96.

R Core Team. 2021. R: a language and environment for statistical computing. R Foundation for Statistical Computing, Vienna, Austria. Available from http://www.r-project.org/.

Rabinowitz, T.R.M., J.T. Lundholm, J.M. Graham, T.M. Bowron, and D. van Proosdij. 2023. Planting techniques and abiotic variation at two salt marsh restoration sites in the Bay of Fundy. *Restoration Ecology* 31: e13707. https://doi.org/10.1111/rec.13707.

Rozalska, K., and S. Coffen-Smout. 2020. Maritimes region fisheries atlas: catch weight landings mapping (2014-2018) on a hexagon grid. *Canadian Technical Report of Fisheries and Aquatic Sciences* 3373: vi + 68 p.

Ruddick, K.G., V. De Cauwer, Y.J. Park, and G. Moore. 2006. Seaborne measurements of near infrared water-leaving reflectance: the similarity spectrum for turbid waters. *Limnology and Oceanography* 51: 1167–1179. https://doi.org/10.4319/lo.2006.51.2.1167.

Ruddick, K.G., F. Ovidio, and M. Rijkeboer. 2000. Atmospheric correction of Sea WiFS imagery for turbid coastal and inland waters. *Applied Optics* 39: 897–912. https://doi.org/10.1364/ao.39.000897.

Schell, T. M. 1998. Compilation of suspended particulate matter (SPM) recorded in the Shepody Bay/Petitcodiac River System. *Canadian Technical Report of Fisheries and Aquatic Sciences* 2246: vii + 29 p.

Siegel, D.A., M. Wang, S. Maritorena, and W. Robinson. 2000. Atmospheric correction of satellite ocean color imagery: the black pixel assumption. *Applied Optics* 39: 3582. https://doi.org/10.1364/ao.39.003582.

Swift, D.J.P., B.R. Pelletier, A.K. Lyall, and J.A. Miller. 1969. Sediments of the Bay of Fundy - a preliminary report. *Atlantic Geology* 5: 95–100. https://doi.org/10.4138/1801.

Tao, J., P.S. Hill, R.P. Mulligan, and P.C. Smith. 2014. Seasonal variability of total suspended matter in Minas Basin, Bay of Fundy. *Estuarine, Coastal and Shelf Science* 151: 169–180. https://doi.org/10.1016/j.ecss.2014.10.005.

Toodesh, R. 2007. The oceanographic circulation of the Port of Saint John over seasonal and tiday time scales. University of New Brunswick.

Virgin, S. D. S., A. D. Beck, L. K. Boone, A. K. Dykstra, J. Ollerhead, M. A. Barbeau, and N. R. McLellan. 2020. A managed realignment in the upper Bay of Fundy: community dynamics during salt marsh restoration over 8 years in a megatidal, ice-influenced environment. *Ecological Engineering* 149: 105713. https://doi.org/10.1016/j.ecoleng.2020.105713.

Wang, M., and W. Shi. 2007. The NIR-SWIR combined atmospheric correction approach for MODIS ocean color data processing. *Optics Express* 15: 15722. https://doi.org/10.1364/OE.15.015722.

Wynne, T.T., M.C. Tomlinson, T.O. Briggs, S. Mishra, A. Meredith, R.L. Vogel, and R.P. Stumpf. 2022. Evaluating the efficacy of five chlorophyll-a algorithms in Chesapeake Bay (USA) for operational monitoring and assessment. *Journal of Marine Science and Engineering* 10: 1104. https://doi.org/10.3390/jmse10081104.

Zions, V. S., B. A. Law, C. O. Laughlin, K. J. Morrison, A. Drozdowski, G. L. Bugden, and S. Roach. 2017. Spatial and temporal characteristics of water column and seabed sediment samples from Minas Basin, Bay of Fundy. *Canadian Technical Report of Fisheries and Aquatic Sciences* 3233: vi + 95 p.